nature metabolism

ARTICLES

https://doi.org/10.1038/s42255-022-00551-7

Check for updates

Macrophages use apoptotic cell-derived methionine and DNMT3A during efferocytosis to promote tissue resolution

Patrick B. Ampomah[1,2] ✉, Bishuang Cai[3], Santosh R. Sukka[1], Brennan D. Gerlach[2], Arif Yurdagul Jr[4], Xiaobo Wang[1], George Kuriakose[1], Lancia N. F. Darville[5], Yan Sun[6], Simone Sidoli[6], John M. Koomen[5], Alan R. Tall[1] and Ira Tabas[1,7,8] ✉

Efferocytosis, the clearance of apoptotic cells (ACs) by macrophages, is critical for tissue resolution, with defects driving many diseases. Mechanisms of efferocytosis-mediated resolution are incompletely understood. Here, we show that AC-derived methionine regulates resolution through epigenetic repression of the extracellular signal-regulated kinase 1/2 (ERK1/2) phosphatase Dusp4. We focus on two key efferocytosis-induced pro-resolving mediators, prostaglandin E_2 (PGE_2) and transforming growth factor beta 1 (TGF-β1), and show that efferocytosis induces prostaglandin-endoperoxide synthase 2/cyclooxygenase 2 (Ptgs2/COX2), leading to PGE_2 synthesis and PGE_2-mediated induction of TGF-β1. ERK1/2 phosphorylation/activation by AC-activated CD36 is necessary for Ptgs2 induction, but this is insufficient owing to an ERK–DUSP4 negative feedback pathway that lowers phospho-ERK. However, subsequent AC engulfment and phagolysosomal degradation lead to Dusp4 repression, enabling enhanced p-ERK and induction of the Ptgs2–PGE_2–TGF-β1 pathway. Mechanistically, AC-derived methionine is converted to S-adenosylmethionine, which is used by DNA methyltransferase-3A (DNMT3A) to methylate Dusp4. Bone-marrow DNMT3A deletion in mice blocks COX2/PGE_2, TGF-β1, and resolution in sterile peritonitis, apoptosis-induced thymus injury and atherosclerosis. Knowledge of how macrophages use AC-cargo and epigenetics to induce resolution provides mechanistic insight and therapeutic options for diseases driven by impaired resolution.

Macrophages play critical roles during the resolution of inflammation by clearing ACs, termed efferocytosis, and secreting pro-resolving factors that mediate tissue repair after injury[1]. Defects in efferocytosis and resolving mediator synthesis lead to cell and tissue necrosis, unresolved inflammation and tissue damage; impaired efferocytosis has been implicated in several chronic inflammatory diseases, including autoimmune diseases, atherosclerosis, chronic lung diseases and neurodegenerative diseases[2,3]. For example, efferocytosis is impaired in advanced atherosclerotic lesions, promoting clinically unstable plaques characterized by necrosis, inflammation and fibrous cap thinning[2,4,5]. Resolving mediators produced during efferocytosis not only promote resolution, but also enhance efferocytosis itself, forming a highly beneficial positive feedback cycle[1,2]. Accordingly, when efferocytosis becomes defective in diseases, impaired resolution ensues as part of a negative feedback cycle[2,3].

Efferocytosis-induced macrophage resolution pathways are triggered by activation of AC receptors or molecules resulting from the phagolysosomal degradation of engulfed ACs[2,3]. For example, AC-derived arginine enhances the engulfment of subsequent ACs via an ornithine–putrescine-dependent metabolic pathway[6]; fatty acids resulting from efferocytosis promote macrophage synthesis of interleukin-10 (IL-10) (ref. [7]); and AC-derived cholesterol activates liver X-receptor mediated resolution pathways[8].

An important efferocytosis-mediated resolution programme involves the synthesis and secretion of PGE_2 and TGF-β1 (ref. [9]). PGE_2 synthesis involves the conversion of arachidonic acid to prostaglandin H_2 by COX2 (encoded by *Ptgs2*), followed by conversion of prostaglandin H_2 to PGE_2 by prostaglandin E synthase (PGES). Although COX2 and PGE_2 have been implicated in inflammation and thrombosis[10,11], their effects are context- and PGE_2 receptor-dependent, and PGE_2 has pro-resolving roles in certain settings, including efferocytosis, atherosclerosis and cardiac ischaemia/reperfusion[9,12–18]. Similarly, although TGF-β can promote inflammation in certain settings, it has potent pro-repair activities[19], including in the settings of efferocytosis and atherosclerosis[9,20].

A key gap in this area of research is how efferocytosis stimulates the production of PGE_2 and TGF-β. In this report, we show that this process occurs through coordinated signalling involving AC-receptor binding and a DNA methylation pathway triggered by AC-derived methionine. Knowledge of this pathway may suggest new therapeutic strategies for the many diseases in which macrophage-mediated resolution is impaired.

Results

Efferocytosis-induced TGF-β1 requires AC degradation and PGE_2. We began by investigating whether the key process of efferocytosis-induced PGE_2 and TGF-β1 (ref. [9]) might be linked

[1]Department of Medicine, Columbia University Irving Medical Center, New York, NY, USA. [2]Novartis Institutes for BioMedical Research, Cambridge, MA, USA. [3]Division of Liver Diseases, Department of Medicine, Icahn School of Medicine at Mount Sinai, New York, NY, USA. [4]Department of Molecular and Cellular Physiology, LSU Health Shreveport, Shreveport, LA, USA. [5]Proteomics and Metabolomics Core, H. Lee Moffitt Cancer Center and Research Institute, Tampa, FL, USA. [6]Department of Biochemistry, Albert Einstein College of Medicine, New York, NY, USA. [7]Department of Pathology and Cell Biology, Columbia University Irving Medical Center, New York, NY, USA. [8]Department of Physiology, Columbia University Irving Medical Center, New York, NY, USA. ✉e-mail: pbampomah1@gmail.com; iat1@columbia.edu

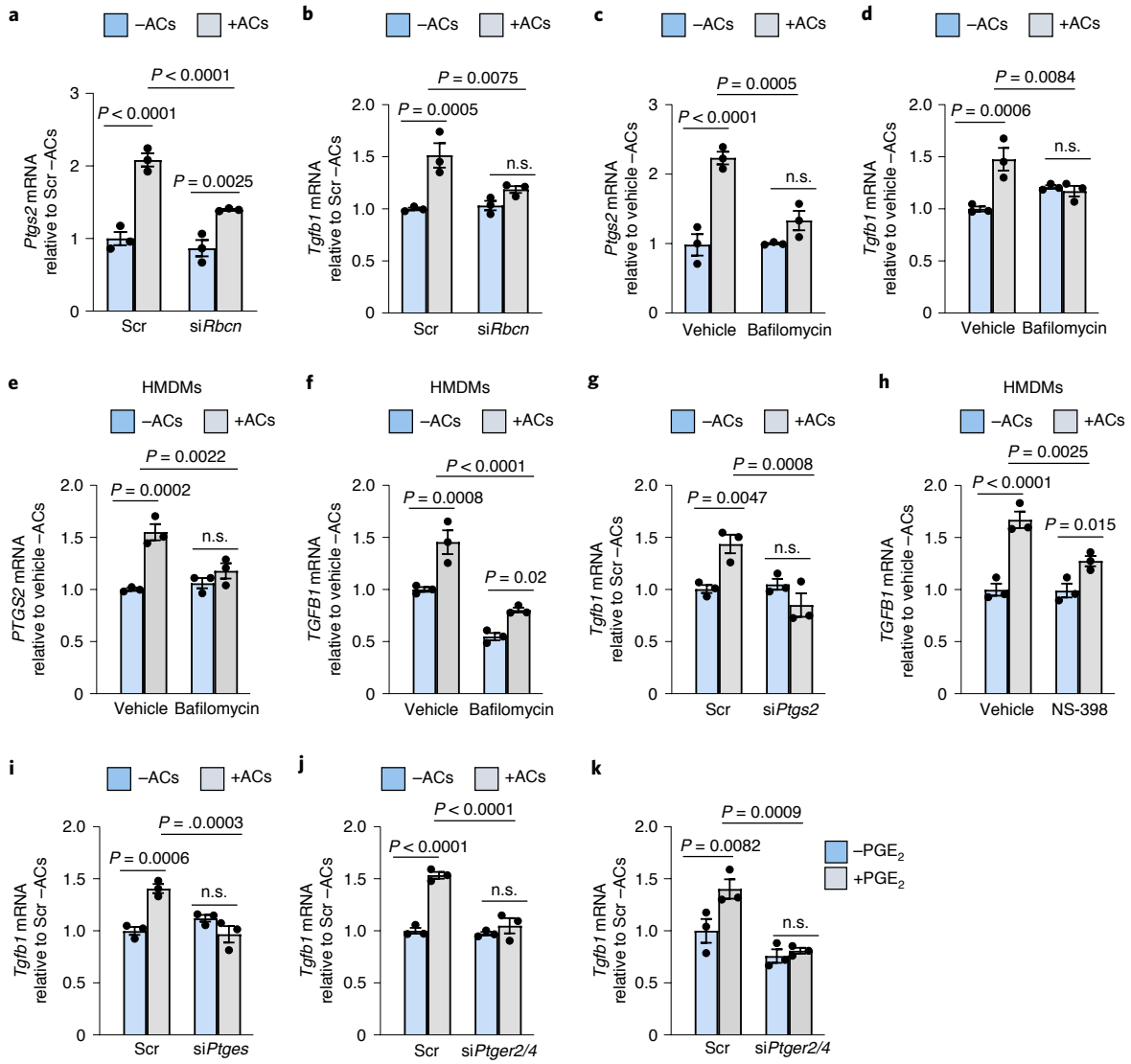

Fig. 1 | Efferocytosis-induced TGF-β1 production requires phagolysosomal AC degradation and Ptgs2/COX2 induction. a–h, BMDMs or HMDMs were pretreated with siRNAs for 72 h or inhibitors for 2 h, as indicated below. The cells were then incubated with (+) or without (–) ACs for 45 min, after which noninternalized ACs were removed by rinsing. After an additional 1 or 6 h of incubation, the cells were assayed for *Ptgs2* or *Tgfb1* mRNA, respectively. **a**,**b**, BMDMs were transfected with scrambled RNA (Scr) or si*Rbcn* and assayed for *Ptgs2* or *Tgfb1*, respectively. **c–f**, BMDMs or HMDMs were pretreated with vehicle or bafilomycin A1. **g**, BMDMs were transfected with Scr or si*Ptgs2*. **h**, HMDMs were pretreated with vehicle or the COX2-specific inhibitor (NS-398). **i**, BMDMs were transfected with Scr or si*Ptges*. **j**, BMDMs were transfected with Scr or si*Ptger2* and si*Ptger4*. **k**, BMDMs were transfected with Scr or si*Ptger2* and si*Ptger4*. After 72 h, the cells were incubated with vehicle or 10 μM PGE_2 for 2 h and then assayed for *Tgfb1* mRNA. The mRNA data are expressed relative to the first control group. Values are means ± s.e.m.; ns, not significant ($P > 0.05$); $n = 3$ biological replicates. Two-sided *P* values were determined by one-way ANOVA with Fisher's LSD post hoc analysis.

to the phagolysosomal degradation of ACs. First, we showed that incubation of bone marrow-derived macrophages (BMDMs) with ACs causes increases in *Ptgs2* messenger RNA, its product COX2, media PGE_2 and media TGF-β1 (Extended Data Fig. 1a–c). The ACs were human Jurkat cells and the primers were based on mouse mRNA sequences, and thus the *Ptgs2* and *Tgfb1* mRNA was from the macrophages, not the engulfed ACs (Extended Data Fig. 1d). To test the importance of AC phagolysosomal degradation, we silenced Rubicon, a protein required for microtubule associated protein 1 light chain 3-associated phagocytosis (LAP) that mediates lysosome–phagosome fusion and phagolysosomal AC degradation during efferocytosis[21]. We found that Rubicon silencing suppressed AC-induced increases in both *Ptgs2* and *Tgfb1* (Fig. 1a,b and Extended Data Fig. 1e). Similar results were found with macrophages pretreated with bafilomycin A1, a lysosomal vacuolar ATPase inhibitor that blocks phagolysosomal AC degradation during efferocytosis[6] (Fig. 1c,d), and with human monocyte-derived macrophages (HMDMs) (Fig. 1e,f). Note that neither si*Rbcn* nor bafilomycin treatment blocked initial AC engulfment (Extended Data Fig. 1f). These data suggest that one or more AC-derived metabolites are involved in the post-efferocytic induction of *Ptgs2*/*Tgfb1*.

On the basis of previous work[22], we hypothesized that AC-induced PGE_2 might induce TGF-β1 in an autocrine/paracrine manner. Consistent with this idea, the AC-induced increase in *Tgfb1* mRNA was prevented by *Ptgs2* silencing in mouse macrophages and by the COX2-specific inhibitor NS-398 (ref. [23]) in HMDMs (Fig. 1g,h and Extended Data Fig. 1g). Incubation of

macrophages with ACs also increased in *Ptges* (PGE synthase), and silencing *Ptges* blocked AC-induced *Tgfb1* mRNA (Fig. 1h,i and Extended Data Fig. 1i). Furthermore, silencing two PGE_2 receptors, EP2 and EP4, decreased AC-induced *Tgfb1*, and exogenous PGE_2 increased *Tgfb1*, which was also blocked by silencing EP2/4 (Fig. 1j,k and Extended Data Fig. 1j,k). By contrast, silencing *Tgfb1* did not affect AC-induced *Ptsg2* (Extended Data Fig. 1l,m). These data suggest that phagolysosomal degradation of ACs triggers *Ptgs2* induction, leading to COX2-mediated PGE_2 synthesis/secretion and then PGE_2-mediated induction of *Tgfb1*.

The pathway uses S-adenosylmethionine from AC-methionine. On the basis of our previous work linking macrophage metabolism of AC-derived amino acids to gene regulation[6], we became interested in methionine, because methionine-derived S-adenosylmethionine (SAM) can be used by histone and DNA methyltransferases to alter gene transcription[24]. Moreover, methionine was among the top ten amino acids showing an increase in macrophages following efferocytosis[6]. SAM is formed by the addition of methionine to ATP, which is catalysed by the enzyme methionine adenosyltransferase 2A (MAT2A)[25]. We observed that treating BMDMs with the MAT2A inhibitor PF-9366 (ref. [26]) or siMat2a blocked AC-induced increases in *Ptgs2* and *Tgfb1* mRNA and TGF-β1 secretion (Fig. 2a,b) without affecting initial AC uptake (Fig. 2a,b and Extended Data Fig. 2a–d). MAT2A inhibition also blocked AC-induced increases in *PTGS2* and *TGFB1* in HMDMs (Fig. 2c,d). Further, exogenously added SAM was sufficient to induce *Ptgs2* and *Tgfb1*, and, as predicted, this was not substantially reduced by PF-9366 (Fig. 2e,f and Extended Data Fig. 2e). Note that the modest trend toward reduction by PF-9366 might be related to a small contribution by the methionine cycle, where SAM is converted to methionine, which can then be converted back to SAM via MAT2A[27].

We further explored the source of methionine in this pathway. First, AC-induced increases in *Ptgs2* and *Tgfb1* were not dependent on methionine in the media (Fig. 2g,h). Next, we sought to trace methionine from AC proteins into macrophage SAM during efferocytosis. Jurkat cells were incubated with $^{13}C_5{}^{15}N$-methionine, labelled with fluorescent PKH26 dye and then rendered apoptotic. To prevent $^{13}C_5{}^{15}N$-SAM formation in Jurkat cells, labelling was done in the presence of the MAT2A inhibitor, and we showed by liquid chromatography tandem mass spectrometry (LC–MS/MS) that the Jurkat cells had $^{13}C_5{}^{15}N$-methionine but not $^{13}C_5{}^{15}N$-SAM (Extended Data Fig. 2f). Macrophages were incubated with these ACs for 45 min, followed by the removal of noninternalized ACs by rinsing and further incubation in medium without ACs for 1 h. The macrophages were then sorted into $PKH26^+$ (AC^+) and $PKH26^-$ (AC^-) cells and analysed by LC–MS/MS for $^{13}C_5{}^{15}N$-SAM. $^{13}C_5{}^{15}N$-SAM was found only in AC^+ macrophages and, importantly, this was markedly inhibited when phagolysosomal hydrolysis was blocked by bafilomycin (Fig. 2i and Extended Data Fig. 2g,h). These combined data provide evidence that methionine originating from phagolysosomal AC degradation during efferocytosis is converted into SAM, which leads to the induction of *Ptgs2* and then PGE_2-mediated induction of *Tgfb1*.

The DNMT3A–PGE_2–TGF-β1 pathway requires DNMT3A. SAM is used by DNA methyltransferases to methylate gene regulatory regions, and thus we investigated whether this process might somehow be involved in the PGE_2–TGF-β1 pathway. We focused on the DNA methyltransferase DNMT3A, which becomes functional in late embryos and after birth[28]. We found that the AC-induced increases in *Ptgs2*, COX2 and *Tgfb1* were blocked in BMDMs from *Dnmt3a*$^{fl/fl}$ *Vav1Cre*$^{+/-}$ mice (haematopoietic (H)-DNMT3A knockout (KO) mice) versus control *Vav1Cre*$^{+/-}$ mice, despite equal uptake of ACs (Fig. 3a–c and Extended Data Fig. 2i,j). Similarly, DNMT3A silencing blocked AC-induced *PTGS2* and *TGFβ1* in HMDMs (Fig. 3d,e and Extended Data Fig. 2k), and the BMDM data were similar when apoptotic macrophages were the source of ACs (Fig. 3f,g). To test another source of cellular methionine cargo, we incubated control and DNMT3A-KO macrophages with immunoglobulin G (IgG)-coated red blood cells (RBCs). By flow cytometry, RBC^+ macrophages had a marked increase in COX2 compared with RBC^- macrophages, and this increase was decreased by ~50% in DNMT3A-KO macrophages (Extended Data Fig. 2l). In contrast to these findings with engulfed cells, control and DNMT3A-KO macrophages, or macrophages treated with scrambled RNA or siDnmt3a, responded similarly to lipopolysaccharide (LPS (*Il6* and *Ptgs2*), interferon-gamma + LPS (COX2 and *Nos2*) and IL-4 (*Arg1*) (Extended Data Fig. 2m–p). Further, basal and AC-induced SAM levels were similar between control and H-DNMT3A-KO macrophages (Extended Data Fig. 2q). Finally, the increases in *Ptgs2* and *Tgfb1* induced by exogenous SAM were also prevented in macrophages lacking DNMT3A (Fig. 3h,i).

The involvement of SAM and DNMT3A prompted us to look at global DNA methylation in efferocytosing macrophages. We found that ACs increased the percentage of 5-methylcytosine (mC) in macrophage DNA, which was partially dampened by MAT2A inhibition or DNMT3A absence (Fig. 3j). We then incubated macrophages with $^{13}C_5{}^{15}N$-methionine-labelled ACs (above) and found that $^{13}CH_3$-DNA, assayed by LC–MS/MS, was detected in macrophages incubated with $^{13}C_5{}^{15}N$-methionine-labelled ACs versus unlabelled ACs, and this was partially blocked by bafilomycin and markedly blocked by bafilomycin plus the MAT2A inhibitor (PF9366) (Extended Data Fig. 2r and Fig. 3k).

As a separate finding, the addition of exogenous PGE_2 did not rescue the defect in *Tgfb1* mRNA in DNMT3A-KO macrophages (Fig. 3l). We then asked whether this finding might be linked to the fact that PGE_2 receptors signal through phosphorylated-CAMP responsive element binding protein 1 (p-CREB1) (ref. [29]). Indeed, PGE_2-induced p-CREB1 was blocked in DNMT3A-KO macrophages (Fig. 3m). Most importantly, silencing CREB1 blocked the increase in *Tgfb1* in macrophages treated with exogenous PGE_2 or incubated with ACs (Fig. 3n,o and Extended Data Fig. 2s). These combined data suggest at least two roles for DNMT3A in efferocytosis-induced pro-resolving mediator production. First, efferocytosis/SAM-mediated *Ptgs2* induction requires DNMT3A, and the finding that methyl groups from AC-derived methionine can be traced to macrophage DNA suggests a possible role for DNA methylation in this pathway (below). Second, the ability of PGE_2 to induce *Tgfb1* also involves DNMT3A via a pathway involving p-CREB1.

The pathway requires DNMT3A-mediated *Dusp4* repression. Because DNA methylation often suppresses gene transcription, we reasoned that suppression of one or more genes by DNA methylation might secondarily increase *Ptgs2*, for example, by removing an inhibitory signal from a *Ptgs2*-inducing pathway. We began with the finding that ERK activation has been implicated in COX2 induction and PGE_2 secretion in other cell types and settings[30]. In addition, we and others have shown previously that TGF-β1 production by macrophages requires ERK1/2 activation[31,32]. Consistent with these previous reports, incubation of macrophages with ACs increased the active form of ERK, p-ERK1/2, which was dampened by bafilomycin (Extended Data Fig. 3a,b). Most importantly, inhibition of ERK1/2 by U0126, or silencing of *Makp1* and *Mapk3*, prevented AC-induced increases in *Ptgs2* and *Tgfb1* and decreased TGF-β1 secretion by mouse and human macrophages (Fig. 4a–d and Extended Data Fig. 3c,d).

ACs are known to activate cell-surface receptors that can activate ERK, notably MerTK and CD36 (refs. [31,33,34]). We therefore targeted these receptors in macrophages, incubated them with PKH-26 or pHrodo-labelled ACs, and conducted flow cytometry assays, gating

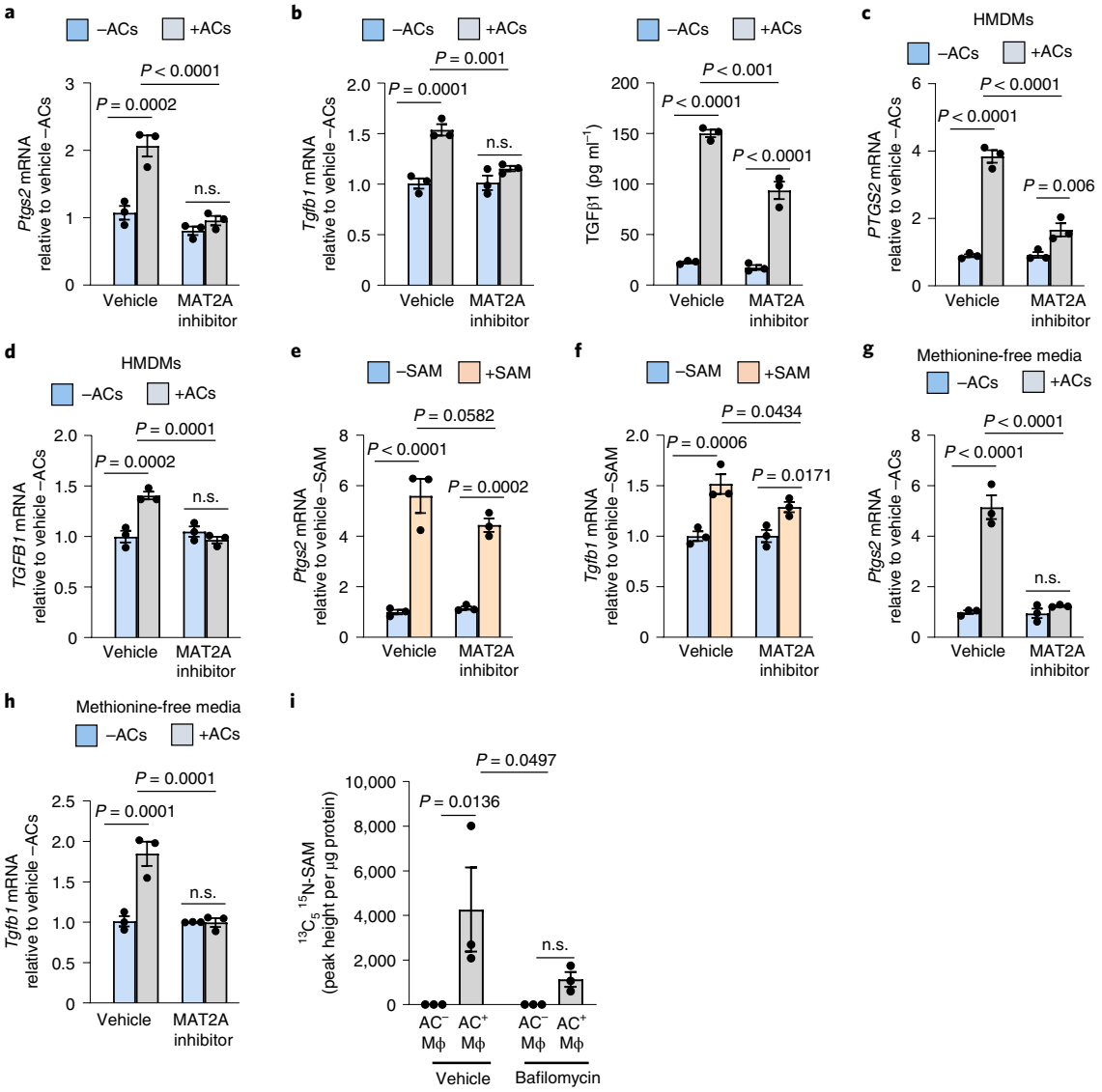

Fig. 2 | The AC-induced Ptgs2-TGF-β1 pathway requires SAM formation from AC-derived methionine. a–d, BMDMs (**a**,**b**) or HMDMs (**c**,**d**) were pretreated with vehicle or the 10 μM MAT2A inhibitor PF-9366 for 2 h. Cells were then incubated with (+) or without (–) ACs for 45 min, after which noninternalized ACs were removed by rinsing. After an additional 1 or 6 h of incubation, the cells were assayed for **a**, *Ptgs2* in BMDMs; **b**, *Tgfb1* in BMDMs; **c**, *TGFB1* in HMDMs; **d**, *PTGS2* in HMDMs. For media TGF-β1 in **b**, macrophages were pretreated for 2 h with vehicle or MAT2A inhibitor before the addition of ACs for 45 min. The macrophages were rinsed to remove nonengulfed ACs and then incubated for an additional 24 h. The cell media were collected and assayed for TGF-β1. **e**,**f**, BMDMs were incubated with vehicle or 20 μM SAM and then assayed for *Ptgs2* after 1 h or *Tgfb1* mRNA after 6 h, respectively. **g**,**h**, BMDMs were cultured in methionine-free DMEM supplemented with dialysed FBS (D-FBS). Before the addition of ACs, cells were pretreated with vehicle or 10 μM MAT2A inhibitor. The cells were then incubated with or without ACs for 45 min, after which noninternalized ACs were removed by rinsing. The cells were assayed for *Ptgs2* after 1 h or *Tgfb1* after 6 h, respectively. **i**, BMDMs were cultured in methionine-free media supplemented with D-FBS. The cells were then pretreated for 2 h with vehicle or bafilomycin A1, followed by incubation for 45 min with PKH26-labelled ACs whose proteins had been labelled with $^{13}C_5{}^{15}N$-methionine before apoptosis induction. After nonengulfed ACs were removed by rinsing and following an additional 1 h of incubation, macrophage extracts were assayed for $^{13}C_5{}^{15}N$-SAM by LC–MS/MS, with the data expressed as peak height per μg of cell protein. The mRNA data are expressed relative to the first control group. Values are means ± s.e.m.; n.s., not significant ($P > 0.05$); $n = 3$ biological replicates. Two-sided *P* values were determined by a one-way ANOVA with Fisher's LSD post hoc analysis.

on labelled AC$^+$ and AC$^-$ macrophages to correct for the lower number of efferocytosing macrophages in receptor-silenced cells. In comparison with AC$^+$ wild-type macrophages, AC$^+$ MerTK-KO macrophages showed a modest decrease in p-ERK and COX2 mean fluorescence intensity (MFI; Extended Data Fig. 3e), while siCD36-treated versus scrambled RNA-treated AC$^+$ macrophages showed a more robust reduction in p-ERK, COX2 and TGF-β1 MFI (Fig. 4e–g and Extended Data Fig. 3f,g). Thus, activation of CD36 by ACs is an important activator of ERK in this pathway.

We next questioned whether ERK activated by the early event of AC binding might be enhanced by DNMT3A after AC engulfment and degradation. Consistent with this idea, control macrophages showed an initial increase in p-ERK1/2 45 min after exposure to ACs, which was maintained after the cells were chased in the absence of ACs for 1 or 2 h (Fig. 4h, blue circles). By contrast, DNMT3A-KO macrophages showed a smaller increase in p-ERK1/2 at 45 min, and the difference between KO and control macrophages persisted for the following 2-h chase period (Fig. 4h, red circles). Based on

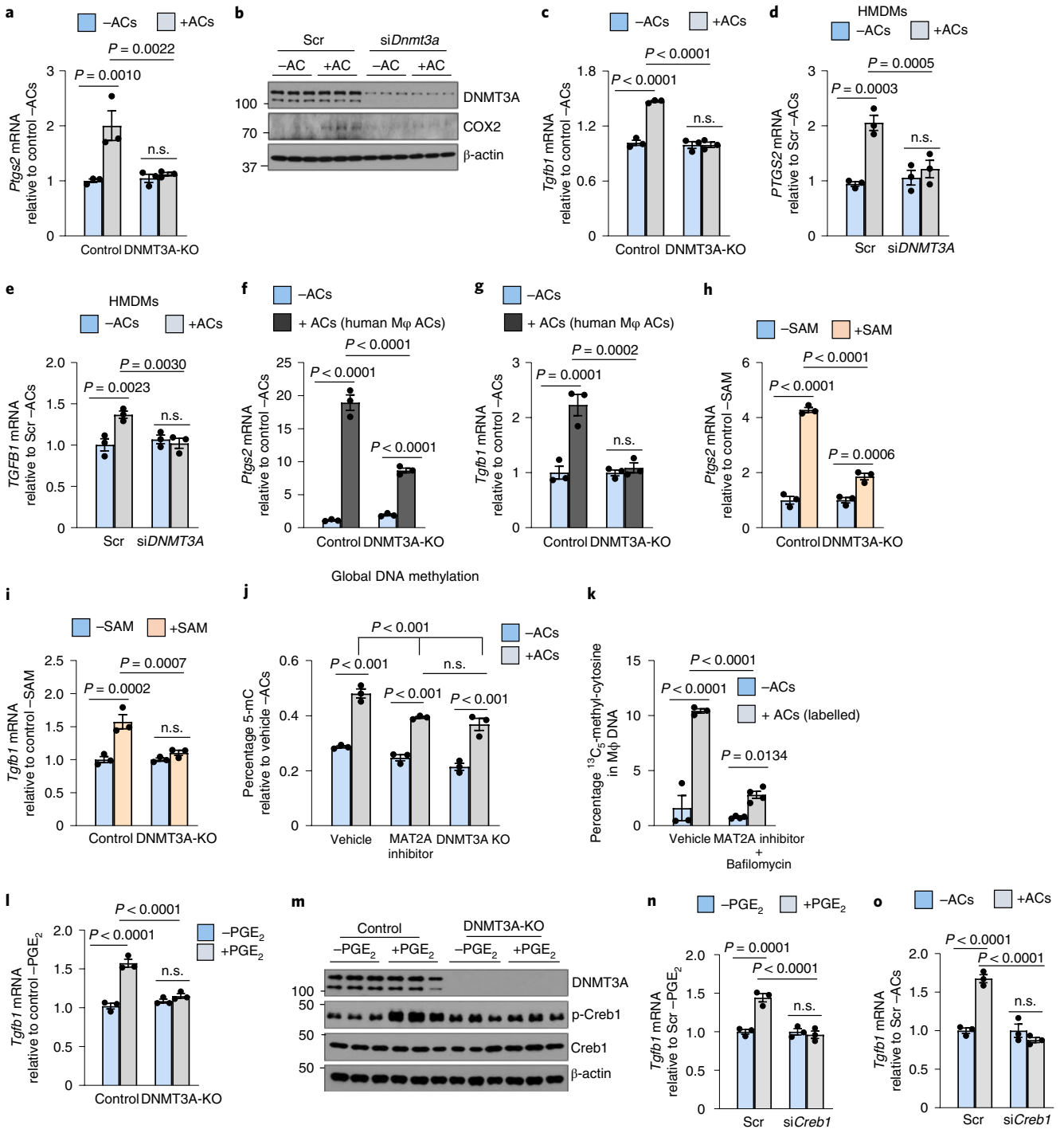

Fig. 3 | The AC-induced COX2-TGF-β1 pathway requires DNMT3A. All incubations with (+) or without (–) ACs were 45 min long, followed by rinsing and then a 1- or 6-h chase period for *Ptgs2* or *Tgfb1*, respectively. **a**, BMDMs from *Vav1Cre*$^{+/-}$ (Control) or *Dnmt3a*$^{fl/fl}$ *Vav1Cre*$^{+/-}$ (H-DNMT3A-KO) mice were incubated with or without ACs and then assayed for *Ptgs2*. **b**, BMDMs treated with scrambled RNA (Scr) or si*Dnmt3a* were incubated with or without ACs and then immunoblotted for DNMT3A, COX2 and β-actin after 3 h. **c**, Control or DNMT3A-KO BMDMs were incubated with or without ACs and then assayed for *Tgfb1*. **d**,**e**, HMDMs treated with Scr or si*DNMT3A* were incubated with or without ACs and then assayed for *PTGS2* or *TGFB1* **f**,**g**, Control or DNMT3A-KO BMDMs were incubated with or without apoptotic human macrophages and then assayed for *Ptsg2* or *Tgfb1*. **h**,**i**, Control or DNMT3A-KO BMDMs were incubated with vehicle or SAM and then assayed for *Ptgs2* after 1 h or *Tgfb1* after 6 h, respectively. **j**, Control macrophages pretreated with vehicle or MAT2A inhibitor (PF9366) and DNMT3A-KO macrophages were incubated with or without ACs and then assayed for global DNA methylation levels (percentage 5-mC). **k**, BMDMs pretreated for 1 h with vehicle or bafilomycin A1 and the MAT2A inhibitor were incubated for 45 min with or without ACs whose proteins were labelled with $^{13}C_5{}^{15}N$-methionine. After rinsing and an additional 1 h of incubation, macrophage DNA was assayed for $^{13}C_5$-mC. **l**, Control or DNMT3A-KO BMDMs were incubated with vehicle or PGE_2 for 2 h and then assayed for *Tgfb1*. **m**, Control or DNMT3A-KO BMDMs were incubated with vehicle or PGE2 for 1 h and then immunoblotted for DNMT3A, p-Creb1, Creb1 and β-actin (1 h). **n**,**o**, BMDMs were pretreated with Scr or si*Creb1* and then incubated ± PGE_2 for 2 h (**n**) or with or without ACs for 45 min followed by a 6-h chase (**o**). The cells were then assayed for *Tgfb1*. The mRNA data are expressed relative to the first control group. Values are means ± s.e.m.; n.s., not significant; $n = 3$ biological replicates. Two-sided *P* values were determined by a one-way ANOVA with Fisher's LSD post hoc analysis.

these data, we hypothesized that DNMT3A might repress a gene that functions to lower p-ERK, for example, an ERK phosphatase. ERK phosphorylation in cells is often transient owing to negative feedback by certain dual-specificity phosphatases (DUSPs), notably DUSP1 and DUSP4 (ref. [35]). We first found that when macrophages were exposed to ACs, there was an increase in *Dusp4* but not *Dusp1* mRNA in siDnmt3a-treated macrophages (Fig. 4i). Similar results with *Dusp4* were found in a time-course experiment comparing control and DNMT3A-KO macrophages (Fig. 4j). In addition, AC-induced Dusp4 was blocked by the ERK inhibitor U0126, consistent with an ERK–DUSP4 negative feedback pathway in these macrophages (Extended Data Fig. 3h). Most importantly, the suppression of *Ptgs2*, COX2 and *Tgfb1* by siDnmt3a or DNMT3A-KO in efferocytosing macrophages was abrogated when Dusp4 was also silenced, but not when Dusp1 was silenced (Fig. 4k,l and Extended Data Fig. 3i–m). Moreover, the reduction in *Tgfb1* expression in si*Mat2a*-treated macrophages was rescued by also silencing Dusp4 (Extended Data Fig. 3n,o). Finally, Dusp4 silencing could not rescue the defect in *Tgfb1* expression in siMapk1/3-treated macrophages (Extended Data Fig. 3p,q), which is consistent with DUSP4 functioning in the pathway by increasing ERK1/2 activation. Finally, using methylated DNA immunoprecipitation, we found that the CpG-rich promoter region of the *Dusp4* gene was methylated in response to ACs in wild-type, but not DNMT3A-deficient macrophages (Fig. 4m). When considered together, the data suggest the following model (Fig. 4n): the initial binding of an AC to an efferocytosis receptor such as CD36 triggers an ERK pathway that induces *Ptgs2*, leading to the downstream COX2–PGE_2–*Tgfb1* pathway. The pathway requires more than transient ERK activation, and thus escape from DUSP4-mediated negative feedback is required. This escape occurs during the next stage in efferocytosis, that is, the phagolysosomal degradation of the engulfed AC, and involves a pathway that relies on AC-methionine, SAM and DNMT3A-mediated suppression of *Dusp4*. Finally, the subsequent ability of PGE_2 to induce *Tgfb1* also involves DNMT3A, which functions through a yet-to-be-defined pathway involving p-CREB1.

Evidence for the DNMT3A–COX2–TGF-β1 pathway in vivo. To test for the presence of the DNMT3A–COX2–TGF-β1 pathway in vivo, we compared control and H-DNMT3A-KO bone marrow-transplanted (BMT) mice (above) using three well-characterized models influenced by macrophage-mediated efferocytosis and resolution: dexamethasone (DEX)-induced thymocyte apoptosis, Zymosan A1-induced peritonitis and atherosclerosis. For the DEX-thymus model, mice were injected with dex to induce thymocyte apoptosis or PBS solution as the vehicle control. In this model, apoptotic thymocytes are continually cleared by thymic macrophages, which is necessary to prevent dead thymocyte accumulation, tissue necrosis and inflammation[6]. We first showed that H-DNMT3A-KO did not affect the initial apoptosis phase, because the number of annexin V^+ (apoptotic) cells in the thymus 4 h after DEX injection was similar in the two groups of mice (Extended Data Fig. 4a). For pathway identification, we examined the thymi from control and H-DNMT3A-KO mice 18 h after the DEX or PBS injection, a time point crucial for identifying macrophage-mediated resolution effects[6]. As designed, DNMT3A was absent in thymic macrophages of the H-DNMT3A-KO mice (Extended Data Fig. 4b, left). We observed that DEX increased thymic macrophage p-ERK, COX2, PGE_2 and TGF-β1 in the control mice, whereas these responses were suppressed in the H-DNMT3A-KO mice (Fig. 5a–c and Extended Data Fig. 4b, right). Importantly, in the DEX-treated cohorts, the thymi of H-DNMT3A-KO mice had higher DUSP4 expression than control mice thymi (Fig. 5d).

In the peritonitis model, Zymosan A1 elicits a neutrophil-mediated sterile inflammatory response, which is followed by a gradual accumulation of efferocytosing macrophages that clear neutrophils as they become apoptotic[36,37]. To test for the presence of the DNMT3A–COX2–TGF-β1 pathway in this model, control and H-DNMT3A-KO mice were injected intraperitoneally with Zymosan A1. After 24 h, but not 12 h, exudate macrophages from the H-DNMT3A-KO mice had decreases in phospho-ERK, COX2 and LAP-TGF-β1 and also in secreted PGE_2 and TGF-β1 (Fig. 5e–g and Extended Data Fig. 4c,d).

To look for the pathway in atherosclerotic lesions, control and H-DNMT3A-KO mice were fed a western-type diet for 12 weeks. As designed, the atherosclerotic lesions of the chimeric knockout mice had undetectable macrophage DNMT3A (Extended Data Fig. 4e). Blood glucose, body weight, total cholesterol and systemic blood parameters were similar in both groups after harvesting (Extended Data Fig. 4f–m). Most importantly, lesional macrophages of H-DNMT3A-KO mice had decreases in p-ERK, COX2 and TGF-β1 (Fig. 5h–j). In summary, DNMT3A-dependent increase in p-ERK, COX2 and TGF-β1 are evident in the macrophages of three different models where macrophage-mediated efferocytosis and resolution are known to play important roles.

The pathway is functional in resolution in vitro and in vivo. PGE_2 and TGF-β1 promote tissue resolution, including efferocytosis, which is an important effector arm of the resolution res ponse[9,12–14,19]. In this context, we reasoned that activation of the DNMT3A pathway by an initial efferocytic event might further promote efferocytosis via autocrine/paracrine effects of TGF-β1. To begin, we confirmed that incubation of macrophages with TGF-β1 in vitro enhances efferocytosis[38], which was blocked by inhibiting transforming growth factor beta receptor I-mediated SMAD

Fig. 4 | The role of ERK, CD36 and DUSP4 in the efferocytosis–Ptgs2/COX2–TGF-β1 pathway. All incubations with (+) or without (–) ACs were 45 min long, followed by rinsing and then a 1- or 6-h chase period for *Ptgs2* or *Tgfb1*, respectively. **a**–**d**, BMDMs (**a**,**b**) or HMDMs (**c**,**d**) pretreated for 2 h with the MEK/ERK inhibitor U0126 were incubated with or without ACs for 45 min and then assayed for **a**, *Ptgs2* in BMDMs; **b**, *Tgfb1* in BMDMs; **c**, *PTGS2* in HMDMs; **d**, *TGFB1* in HMDMs. Media TGF-β1 was assayed 24 h after AC removal. **e**–**g**, BMDMs treated with scrambled RNA (Scr) or si*Cd36* were incubated with PKH26-labelled ACs for 45 min and then assayed by flow cytometry for p-ERK1/2 MFI, or, after an additional 3 or 18 h of incubation, for COX2 or TGF-β1 MFI, respectively, gating on $PKH26^+$ (AC^+) and $PKH26^-$ (AC^-) macrophages. **h**, Control and DNMT3A-KO BMDMs were incubated with PKH26-labelled ACs for 45 min and then assayed by flow cytometry for p-ERK1/2 at the indicated time points after AC removal. **i**, BMDMs transfected with Scr or si*Dnmt3a* were incubated with or without ACs for 45 min, chased for 1 h and then assayed for *Dusp1* or *Dusp4*. **j**, Control or DNMT3A-KO BMDMs were incubated with or without ACs and then assayed for *Dusp4* mRNA after 0 or 1-h chase. **k**,**l**, BMDMs treated with Scr, si*Dnmt3a*, si*Dusp4* or si*Dnmt3a* + si*Dusp4* were incubated with or without ACs and then assayed for *Ptgs2* after 1 h or *Tgfb1* after 6 h, respectively. **m**, Control or DNMT3A-KO BMDMs were incubated with or without ACs and then after 1 h subjected to methylated DNA immunoprecipitation to immunoprecipitate fragments of methylated DNA. PCR targeting the CpG-rich region of the *Dusp4* promoter was used to determine the fold-enrichment of methylated DNA relative to IgG control. **n**, Pathway scheme, showing AC-CD36-mediated ERK activation, which is limited by Dusp4, and the subsequent AC-degradation pathway, which represses Dusp4 via DNMT3A-mediated DNA methylation to sustain p-ERK. The pathway leads to PGE_2, which acts via EP2/4 and p-CREB to induce *Tgfb1*. The p-CREB pathway also involves DNMT3A. The data in **a**–**l** are expressed relative to the first control group. Values are means ± s.e.m.; n.s., not significant; $n = 3$ biological replicates. Two-sided *P* values were determined by one-way ANOVA with Fisher's LSD post hoc analysis.

phosphorylation with LY3200882 (Extended Data Fig. 5a). More importantly, incubation of macrophages with conditioned media (CM) from AC-exposed control macrophages, but not AC-exposed DNMT3A-KO macrophages, increased efferocytosis, and the increase seen with control-macrophage CM was blocked by an anti-TGF-β1 antibody (Fig. 6a). These data are consistent with the

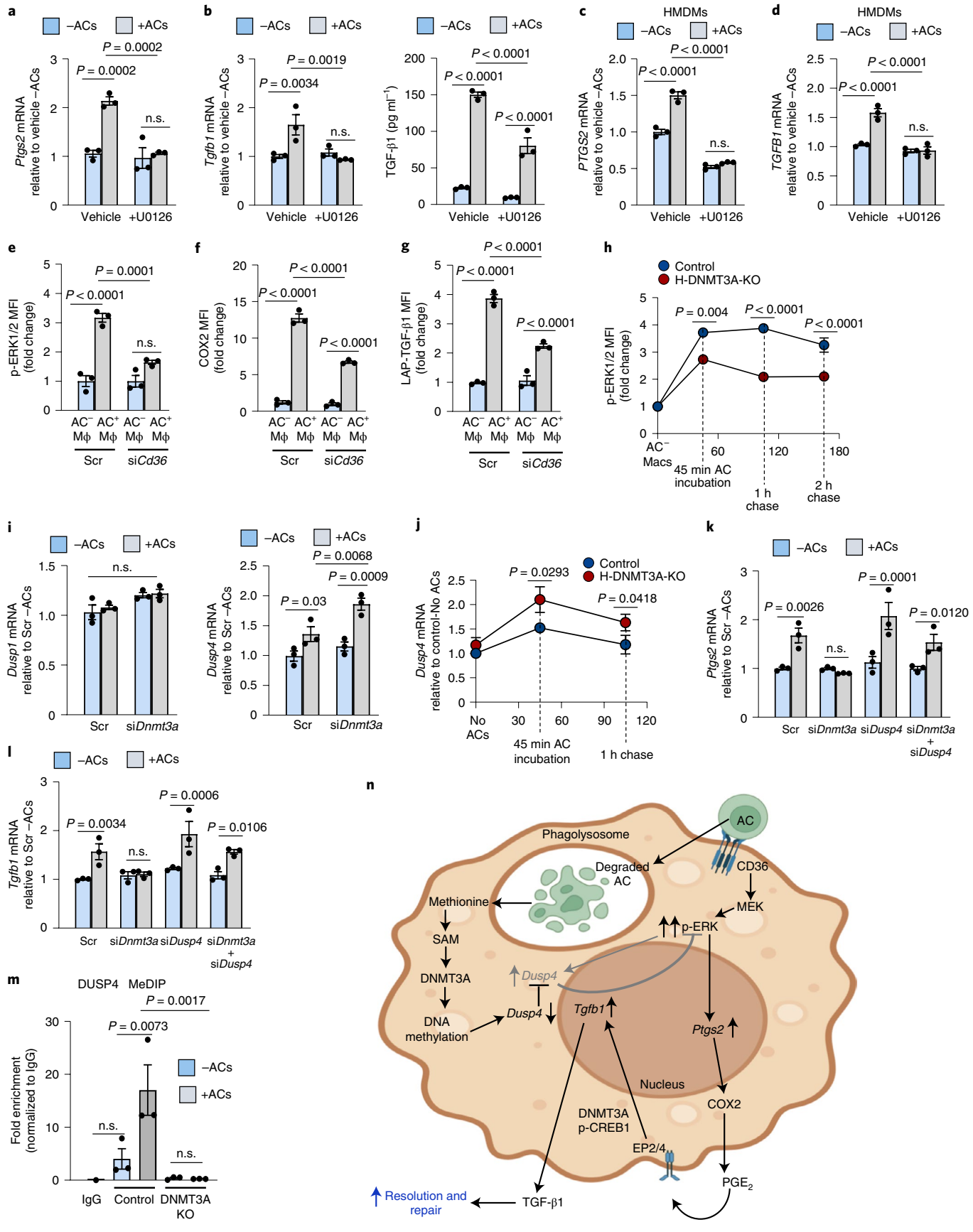

idea that efferocytosis-induced TGF-β1 secretion further increases efferocytosis by a paracrine mechanism.

To test the functionality of this pathway in vivo, we turned to the DEX-thymus model and looked for signs of impaired efferocytosis and resolution in the H-DNMT3A-KO cohort. As alluded to above, within 4 h of DEX treatment, there is marked thymocyte apoptosis, but after 18 h the number of apoptotic thymocytes is modest owing to their clearance by thymic macrophages[6]. Accordingly, although there was a modest increase in ACs in the thymi of the control mice 18 h after DEX, thymus weight and cellularity were decreased owing to macrophage-mediated clearance of apoptotic thymocytes (Fig. 6b,c and Extended Data Fig. 5b, groups 1 and 3). Most importantly, the thymi of the H-DNMT3A-KO cohort showed a greater increase in ACs and cellularity and a smaller decrease in thymus weight after DEX, indicative of impaired continual efferocytosis (Fig. 6b,c and Extended Data Fig. 5b, groups 2 and 4). To assess efferocytosis directly, we stained thymic sections in the DEX-treated cohorts for macrophages using anti-Mac2 antibody and TdT-mediated dUTP-X nick end labeling (TUNEL) to mark dead thymocytes and then quantified the ratio of macrophage-associated TUNEL$^+$ cells to free TUNEL$^+$ cells as a measure of efferocytosis[6]. Note that 'macrophage-associated TUNEL$^+$ cells' refers to macrophages with cytoplasmic TUNEL$^+$ living macrophages, not nuclear-TUNEL$^+$ dead macrophages, which are extremely rare in this model (Extended Data Fig. 5c). We observed that the ratio of macrophage-associated to free TUNEL$^+$ thymocytes was lower in the thymi of DEX-treated H-DNMT3A-KO versus DEX-treated control mice (Fig. 6d), with similar levels of thymic macrophages (Extended Data Fig. 5d), further supporting a defect in efferocytosis.

ACs become necrotic when they remain uncleared. As such, we examined sections from PBS and DEX-treated control and H-DNMT3A-KO mice for evidence of necrosis in sections stained with haematoxylin and eosin. As expected, there was no observable difference between the control and KO groups after PBS treatment, but 18 h after DEX, the KO cohort showed a greater increase in per cent necrosis than the control cohort (Fig. 6e). Further, the thymi of DEX-treated H-DNMT3A-KO mice had a higher level of immunoreactive tumour necrosis factor-alpha and a trend toward higher IL-6 compared with the thymi of DEX-treated control mice (Extended Data Fig. 5e,f). Thus, in the DEX-thymus model, haematopoietic DNMT3A deletion impairs efferocytosis and resolution, which, when considered together with the decreases in COX2 and TGF-β1 in this model shown in the previous section, provide evidence for the functionality of the DNMT3A–COX2–TGF-β1 pathway in vivo.

We next examined the Zymosan sterile peritonitis model. Peritoneal polymorphonuclear cell (PMN) counts were similar between control and H-DNMT3A-KO mice during the inflammatory stage at 12 h, but the KO cohort showed a relatively impaired decrease in PMNs compared with the control cohort at both 24 and 48 h (Fig. 6f). We also showed in a separate experiment that the exudate PMN numbers were also different between the two cohorts at 18 h after Zymosan (Extended Data Fig. 5g). On the basis of previous studies using this model[36,37], this finding suggests that loss of DNMT3A in macrophages impairs resolution in sterile peritonitis and probably compromises the efferocytic clearance of apoptotic PMNs by exudate macrophages. Following this observation, we determined whether intraperitoneal (i.p.) injection of TGF-β1, whose production is impaired in DNMT3A-deficient mice after injection of Zymosan (above), would restore efferocytosis and resolution. As an initial test, we first showed that injection of wild-type mice with 200 ng of TGF-β1 i.p. 15 and 20 h after Zymosan lowered exudate PMN number 24 h later (Extended Data Fig. 5h), which is consistent with the above in vitro data showing that TGF-β1 enhances efferocytosis. Most importantly, we found that treatment of H-DNMT3A-KO mice with TGF-β1 15 and 20 h after Zymosan lowered the number of PMNs to the level seen in the control cohort (Fig. 6g). We then immunostained cells from the peritoneal exudate for the neutrophil marker Gr1 and the macrophage marker F4/80 and used flow cytometric analysis to evaluate the percentage of macrophages (F4/80$^+$ cells) with internalized PMNs (F4/80$^+$Gr1$^+$ cells), which is an indicator of in vivo efferocytosis[33]. TGF-β1 treatment in H-DNMT3A cohort increased the percentage of efferocytosing macrophages (F4/80$^+$Gr1$^+$) to the level seen in the control chimeric cohort (Fig. 6h). Thus, as in the DEX-thymus model, H-DNMT3A-KO impairs resolution and efferocytosis, with direct evidence for the role of TGF-β1 in this model.

Lastly, we examined the 12-week atherosclerosis model, focusing on the TGF-β1-mediated endpoints of fibrous cap thickness and efferocytosis, both of which are features of plaque resolution and stability[2,4,5,20,39]. H-DNMT3A-KO resulted in marked decreases in cap thickness when compared with lesions from control mice (Fig. 6i). Importantly, this finding was not simply a reflection of smaller lesion size (Fig. 6j), because lesion size was not affected by H-DNMT3A-KO (Extended Data Fig. 5i). Moreover, lesional efferocytosis was impaired in the lesions of H-DNMT3A-KO versus control mice (Fig. 6k). Thus, in this complex, disease-relevant model, there is evidence that the DNMT3A pathway plays a role in processes linked to resolution and efferocytosis.

Discussion

A fascinating concept that has emerged in the area of inflammation resolution relates to the ability of macrophages to use molecules derived from the phagolysosomal hydrolysis of ACs to drive resolution and continual efferocytosis[6–8]. Thus far, the mechanisms have focused on AC metabolite-induced pathways that result in specific transcription factor activation, mRNA stabilization or cellular energy metabolism alteration[6–8]. Here we report on a new mechanism that involves epigenetic gene regulation. In this case, AC-derived methionine is converted to SAM, which provides the substrate for DNMT3A-mediated DNA methylation. The result is methylation-induced suppression of *Dusp4*, which enables prolonged ERK phosphorylation to induce *Ptgs2* and subsequent activation of the PGE_2–TGF-β1 resolution pathway (Fig. 4n). This

Fig. 5 | Evidence for the DNMT3A–COX2–TGF-β1 pathway in vivo. a–d, Wild-type (WT) C57BL/6J mice were transplanted with BM from *Vav1Cre*$^{+/-}$ (Control) or *Dnmt3a*$^{fl/fl}$ *Vav1Cre*$^{+/-}$ (H-DNMT3A-KO) mice and injected 4 weeks later with PBS or DEX. After 18 h, the thymi were harvested and immunostained for Mac2 (macrophages) and the following proteins: (**a**) p-ERK1/2, $n=4$; (**b**) COX2, $n=4$; (**c**) TGF-β1, $n=4$; and (**d**) DUSP4, $n=4$. The data are quantified as MFI per Mac2$^+$ area, expressed relative to the first control group. Scale bars, 50 μm. **b** and **c** show the content of PGE_2 and TGF-β1, respectively, in thymic extracts as assayed by ELISA ($n=3$ and 4 for PBS and DEX groups respectively). **e–g**, Control or H-DNMT3A-KO BMT mice were injected i.p. with 1 mg ml^{-1} Zymosan A1. After 24 h, peritoneal exudate cells were analysed by flow cytometry for the following proteins, gating on F4/80$^+$ cells (macrophages): (**e**) p-ERK, $n=4$; (**f**) COX2, $n=4$; (**g**) LAP-TGF-β1, $n=4$. **f** and **g** also show the content of PGE_2 ($n=8$) and TGF-β1 ($n=8$), respectively, in peritoneal exudates as assayed by ELISA. **h–j**, *Ldlr*$^{-/-}$ (LDLR-KO) mice were transplanted with bone marrow from *Vav1Cre*$^{+/-}$ (Control) or *Dnmt3a*$^{fl/fl}$ *Vav1Cre*$^{+/-}$ (H-DNMT3A-KO) and, after 4 weeks, fed a western-type diet for 12 weeks. Aortic root sections were immunostained for Mac2 and the following proteins: (**h**) p-ERK1/2, $n=7$; (**i**) COX2, $n=7$; and (**j**) TGF-β1, $n=7$. The data are quantified as MFI per Mac2$^+$ area expressed relative to the control group. Scale bars, 50 μm. Values are means ± s.e.m., n.s., not significant ($P>0.05$). Two-sided *P* values were determined by the Student's *t*-test for two groups or one-way ANOVA with Fisher's LSD post hoc analysis for four groups.

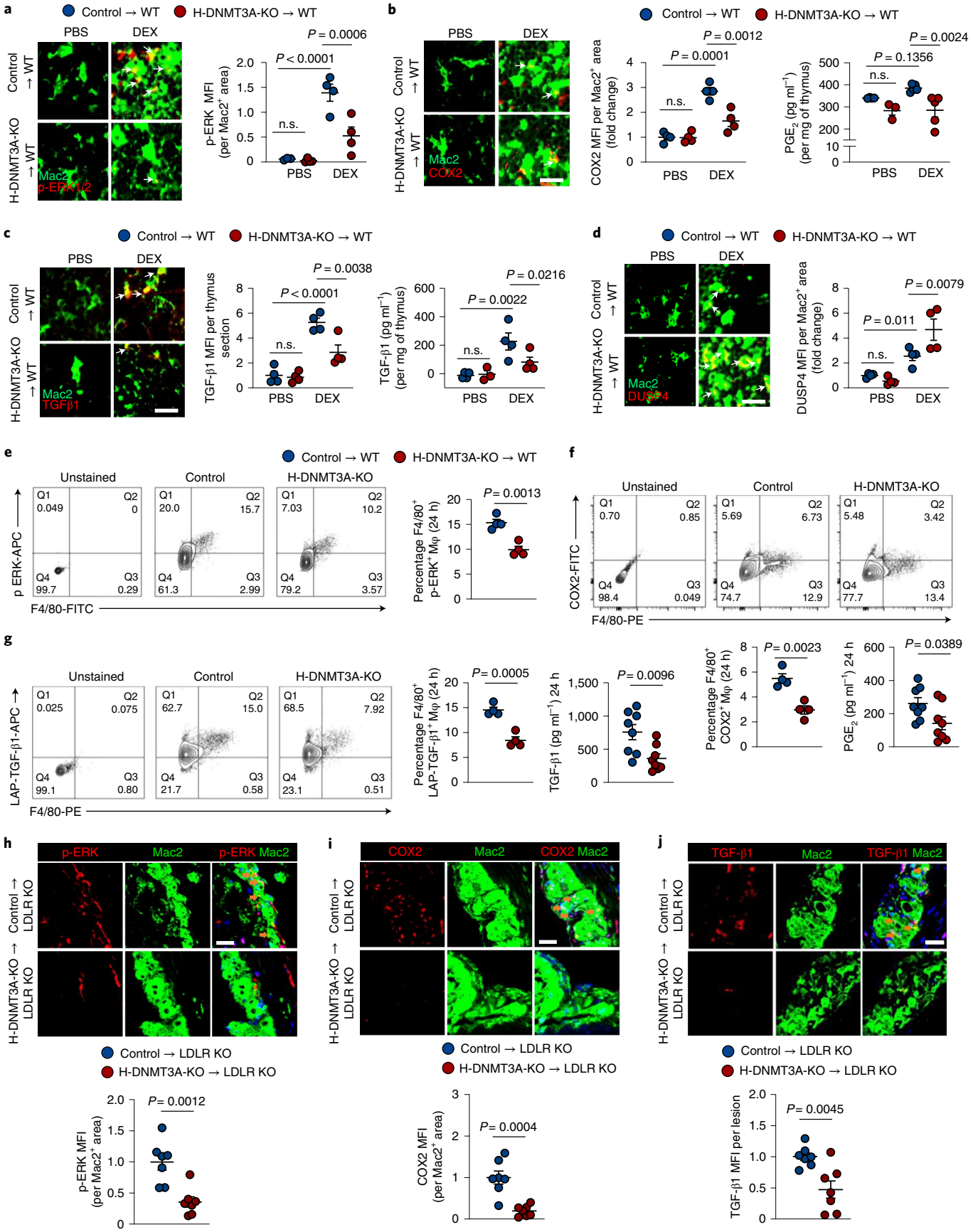
a
Control → WT
H-DNMT3A-KO → WT
PBS
DEX
Control → WT
H-DNMT3A-KO → WT
Mac2
p-ERK1/2
p-ERK MFI (per Mac2+ area)
P = 0.0006
P < 0.0001
n.s.
b
Mac2
COX2
COX2 MFI per Mac2+ area (fold change)
P = 0.0012
P = 0.0001
PGE2 (pg ml−1) (per mg of thymus)
P = 0.0024
P = 0.1356
c
Mac2
TGFβ1
TGF-β1 MFI per thymus section
P = 0.0038
P < 0.0001
TGF-β1 (pg ml−1) (per mg of thymus)
P = 0.0216
P = 0.0022
d
Mac2
DUSP4
DUSP4 MFI per Mac2+ area (fold change)
P = 0.0079
P = 0.011
e
Unstained
Control
H-DNMT3A-KO
p ERK-APC
F4/80-FITC
Percentage F4/80+ p-ERK+ Mφ (24 h)
P = 0.0013
f
COX2-FITC
F4/80-PE
g
LAP-TGF-β1-APC
F4/80-PE
Percentage F4/80+ LAP-TGF-β1+ Mφ (24 h)
P = 0.0005
TGF-β1 (pg ml−1) 24 h
P = 0.0096
Percentage F4/80+ COX2+ Mφ (24 h)
P = 0.0023
PGE2 (pg ml−1) 24 h
P = 0.0389
h
p-ERK
Mac2
p-ERK Mac2
Control → LDLR KO
H-DNMT3A-KO → LDLR KO
p-ERK MFI (per Mac2+ area)
P = 0.0012
i
COX2
COX2 Mac2
COX2 MFI (per Mac2+ area)
P = 0.0004
j
TGF-β1
TGF-β1 Mac2
TGF-β1 MFI per lesion
P = 0.0045

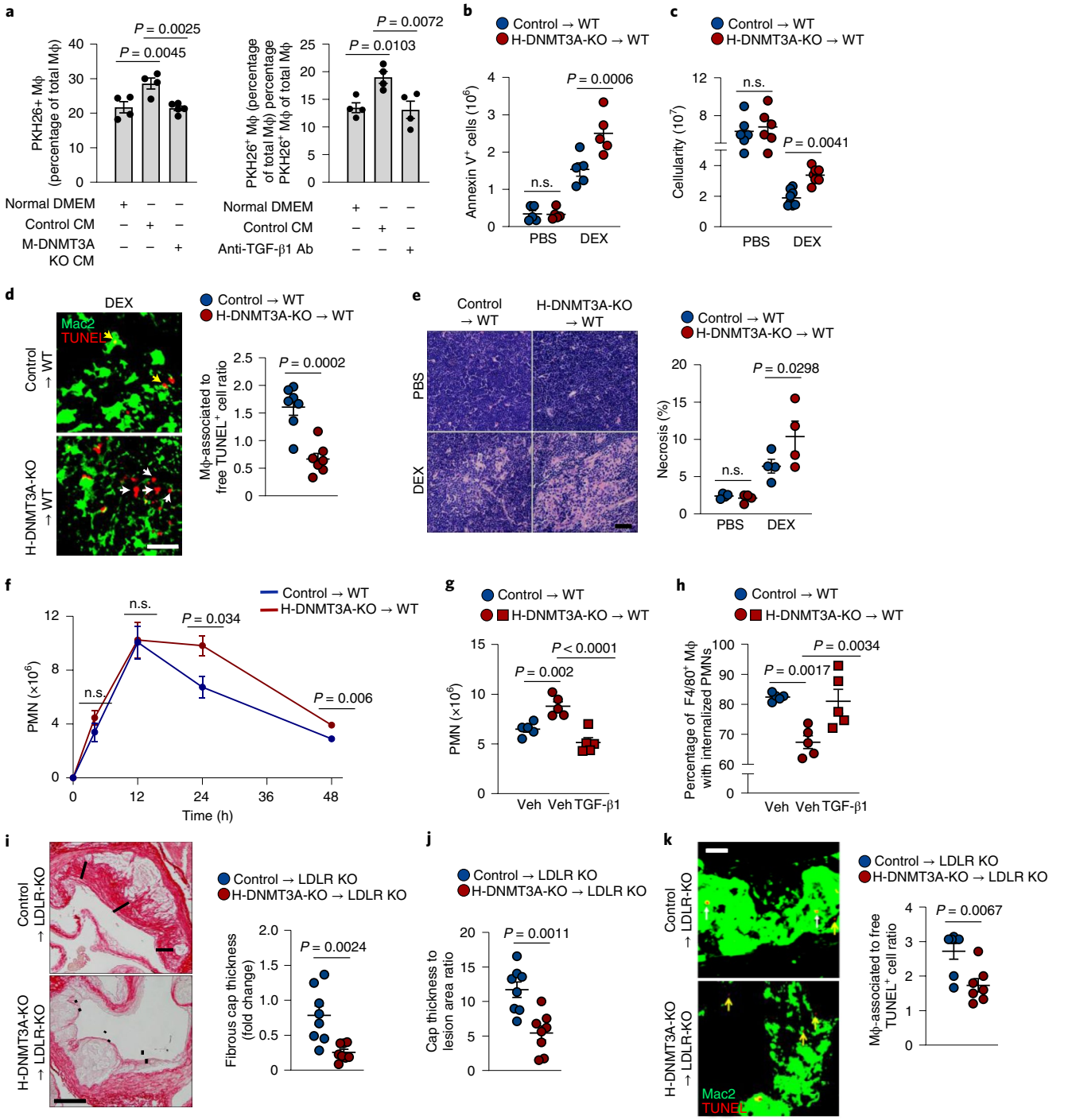

Fig. 6 | Loss of haematopoietic cell DNMT3A impairs efferocytosis in vitro and resolution in vivo. a, Eighteen-hour CM from control or DNMT3A-KO BMDMs incubated with (+) or without (–) AC, or DMEM control, were added to recipient BMDMs (left). In a parallel experiment (right), CM from control BMDMs were treated with or without anti-TGF-β1 antibody and then added to BMDMs. After 1 h, the BMDMs were incubated with or without PKH26 labelled ACs and then assayed for per cent PKH26-AC$^+$ of total macrophages ($n = 4$ biological replicates). **b**–**e**, The thymi of PBS and DEX-treated control and H-DNMT3A-KO BMT mice similar to those in Fig. 5a–d were assayed for annexin V$^+$ cells, $n = 5$ mice/group (**b**); cellularity, $n = 6$ (PBS) and 8 (DEX) mice (**c**); efferocytosis, $n = 7$ mice/group; yellow and white arrows indicate macrophage-associated or free TUNEL$^+$ cells, respectively (**d**); and per cent necrosis, $n = 4$ mice/group (**e**). Scale bars, 50 μm (**d**) and 200 μm (**e**). **f**, The peritoneal exudates of Zymosan A1-injected control and H-DNMT3A-KO BMT mice similar to those in Fig. 5e–g were assayed for Ly6G$^+$ PMN as a function of time after Zymosan A1 injection, $n = 5$ mice/group. **g**,**h**, As in **f**, but a cohort of KO mice received 200 ng ml^{-1} TGF-β1 i.p., whereas control and KO mice received vehicle (Veh). After 24 h, the exudates were assayed for the number of PMNs, $n = 5$ mice/group (**g**), and for the percentage of F4/80$^+$ macrophages that were Gr1$^+$ by flow cytometry (efferocytosis of PMNs), $n = 5$ mice/group (**h**). **i**–**k**, For control and H-DNMT3A-KO BMT *Ldlr*$^{-/-}$ mice fed a western-type diet for 12 weeks, similar to those in Fig. 5h–j, aortic root lesions were assayed for fibrous cap thickness, expressed relative to the control cohort, $n = 8$ mice/group (**i**); fibrous cap thickness as a ratio of the lesion area, $n = 8$ mice/group (**j**); and efferocytosis, $n = 7$ mice/group (**k**). Scale bar, 200 μm (**i**) and 50 μm (**k**). For **k**, yellow and white arrows indicate macrophage-associated (top) or free TUNEL$^+$ (bottom) cells, respectively. Values are means ± s.e.m., n.s., not significant. Two-sided *P* values were determined by the Student's *t*-test for two groups or one-way ANOVA with Fisher's LSD post hoc analysis for four groups.

pathway is supported by mechanistic data using BMDMs and HMDMs; by the presence of the unique biochemical signature of the pathway in resolution settings in vivo; and, most importantly, by DNMT3A-causation experiments in vivo in settings where macrophage-mediated efferocytosis and resolution are important, notably, atherosclerosis. We showed that DNMT3A-KO or silencing in efferocytosing macrophages suppresses the incorporation of methyl groups from AC-methionine into SAM and DNA, and decreases *Dusp4* promoter methylation. However, future studies are needed to show that AC-derived methionine per se is the source of methyl groups on the *Dusp4* promoter and that methylation of this promoter is directly responsible for AC-induced repression of *Dusp4* expression.

The major premise for the study was that efferocytosis promotes resolution by stimulating the synthesis and secretion of PGE_2 and TGF-β1 (ref. [9]) Moreover, another study showed that a CD36-activating antibody led to the induction of TGF-β1 in a leukaemia-derived macrophage cell line[31]. Our studies in BMDMs and HMDMs indicate that AC-induced activation of CD36-ERK1/2 is limited by a DUSP4-mediated negative feedback pathway and that PGE_2 and TGF-β1 induction requires *Dusp4* repression via the subsequent step of AC engulfment and phagolysosomal degradation. Other efferocytosis receptor-ERK pathways may have a more modest role than CD36, as demonstrated by our data with MerTK-KO macrophages.

Our data suggest that methionine/SAM is rate-limiting for at least certain DNA methylation events in macrophages and that AC-derived methionine, or exogenous SAM, provides the necessary substrate for DNA methylation. Other DNA and histone methylation reactions that are known to be active in differentiating macrophages[40] may deplete local stores of endogenous SAM, which could contribute to the rate-limiting property of AC-derived methionine/SAM. Previous examples suggesting that methionine may be rate-limiting in DNA methylation-dependent processes include the use of exogenous methionine by T cells to expand the Th17 lineage[41] and by macrophages to inhibit LPS-induced inflammation[42]. In theory, it is also possible that efferocytosis increases the enzymatic activity of DNMT3A methyltransferase, for example, by suppressing negative regulatory processes that limit DNMT3A activity[43,44].

Our findings raise the possibility that enhancers or promoters in addition to the *Dusp4* promoter are methylated in efferocytosing macrophages, leading to changes in the expression of other genes. Global methylation analysis coupled with assay for transposase-accessible chromatin using sequencing and RNA sequencing in control and DNMT3A-knockout macrophages incubated with or without ACs will help shed light on this issue. In a more general sense, the actions of other DNA methyltransferases and/or histone methyltransferase[45] may also be stimulated by postefferocytotic SAM formation, leading to yet additional changes in gene expression following the uptake and degradation of ACs. Finally, prolonged ERK activation in efferocytosing macrophages caused by *Dusp4* repression is likely to have effects beyond *Ptgs2* induction, and elucidation of these may reveal additional insight into postefferocytosis resolution signalling.

Advanced atherosclerosis was one of the models we used to show that the DNMT3A pathway is present and functional in vivo. Human and experimental advanced atherosclerotic lesions are associated with impaired resolution, and molecular–genetic and pharmacological studies in mice have shown that impaired resolution contributes to plaque progression, whereas pharmacological restoration of resolution suppresses plaque progression[2,4,5,20,39,46,47]. We showed here that homozygous deletion of haematopoietic DNMT3A led to fibrous cap thinning and impaired efferocytosis, two features of unstable plaques in humans that we predicted would occur via the suppression of TGF-β1 synthesis[9,19,20]. Moreover, the lower expression level of $COX2/PGE_2$ in haematopoietic DNMT3A-deficient mice may contribute to the overall defect in resolution, because $COX2/PGE_2$ has been implicated in several anti-inflammatory responses[9,12–14,48]. Furthermore, experimental atherosclerotic mouse models have revealed a direct role of COX2 in protecting against lesion development and suppressing pro-inflammatory IL-6 and tumour necrosis factor-alpha production[15–18]. Age-related loss-of-function somatic mutations in *DNMT3A* in humans (clonal haematopoiesis of indeterminate potential (CHIP)) are associated with an increased incidence of coronary artery disease (CAD)[49], with the mechanism remaining unknown. Thus, a topic for future study will be to determine if the degree of DNMT3A lowering in CHIP is enough to compromise the DNMT3A–PGE_2–TGF-β1 pathway in atherosclerotic lesional macrophages, thus providing at least one mechanism linking *DNMT3A* CHIP to CAD. This mechanism may be relevant to a common dominant-negative *DNMT3A* CHIP mutation associated with CAD, $DNMT3A^{R882H}$. In addition, the findings from this study might be particularly applicable to atherosclerosis regression, where efferocytosis and resolution play important roles in plaque stabilization[6,50]. Finally, conceiving ways to therapeutically enhance the DNMT3A–PGE_2–TGF-β1 pathway may provide a new way to boost resolution in atherosclerosis and other key diseases in which resolution is impaired. In this context, our findings may provide a mechanistic basis to an emerging area in resolution therapeutics in which infusion of ACs, including apoptotic mesenchymal stems cells, is used to trigger efferocytosis-mediated resolution pathways[51]. This type of therapy is effective in experimental models of autoimmune disease and has been shown in a small clinical trial to decrease the incidence of graft-versus-host disease in subjects receiving haematopoietic stem cell transplantation for haematologic malignancies[51,52]. Several studies have suggested that stimulation of PGE_2 secretion by efferocytosing macrophages may be an important pro-resolving mechanism of this therapeutic strategy[53,54] and, based on the findings here, this process may be linked to TGF-β1 secretion as well. To the extent that infusion of ACs may cause adverse effects, that is, if the infused cells become necrotic[51], knowledge of the DNMT3A–PGE_2–TGF-β1 pathway may suggest alternative, safer strategies to enhance resolution in disease settings.

Methods

Experimental animals. Animal protocols used for experiments were approved by Columbia University's Institutional Animal Care and Use Committee and animals were cared for according to National Institutes of Health (NIH) guidelines for the care and use of laboratory animals under protocol number AAAY9450. The mice were housed socially in standard cages at 22 °C and under a 12:12 h light/dark cycle in a barrier facility with ad libitum access to water and food. Eight-week-old male C57BL/6J wild-type mice (Jackson Laboratory, strain 000664) were used as BMT-recipient mice for the DEX-thymus and Zymosan A1 experiments, with n numbers indicated in the figure legends. Eight-week-old male LDLR-KO mice on the C57BL/6J background (B6.129S7-*Ldlr*$^{tm1Her/J}$; Jackson Laboratory, strain 002207) were used as BMT-recipient mice for the atherosclerosis experiments, with n numbers indicated in the figure legends. All purchased mice were allowed to adapt to housing in the animal facility for 1 week before the commencement of experiments. For BMT donor mice, we used 8-week-old *Dnmt3a*$^{fl/fl}$*Vav1Cre*$^{+/-}$ and *Vav1Cre*$^{+/-}$ control male mice, both on the C57BL/6J background, which were a gift from S. Mukherjee and A. Burke. The ratio of donor to recipient mice for BMT was 10:1. *Mertk*$^{fl/fl}$ *Lyz2cre* male mice on the C57BL/6J background were generated as previously described[55] and used at 8 weeks of age. Investigators were blinded for atherosclerosis experiments, but were not for experiments from the DEX-induced thymocyte apoptosis model and Zymosan-induced peritonitis model.

Generation of BMDMs. Bone marrow (BM) cells from either male or female 8–12-week-old mice were cultured in DMEM supplemented with 10% heat-inactivated FBS, 100 mg ml^{-1} streptomycin,10 U ml^{-1} penicillin and 20% L-929 fibroblast-CM for 6–8 d, after which they were ready for use in the experiments.

Generation of HMDMs. Peripheral human blood leucocytes were isolated from buffy coats of anonymous, de-identified healthy adult volunteers, with informed consent (New York Blood Center). The leucocytes were purified in a discontinuous gradient of Histopaque solution and added to 24-well tissue culture plates in a humidified CO_2 incubator at 37 °C. After 4 h to allow for adhesion, the monolayers were rinsed to remove unattached cells, and the medium was changed to

RPMI-1640 (Gibco) containing 10% heat-inactivated FBS, 100 mg ml^{-1} streptomycin, 10 U ml^{-1} penicillin and 20 ng ml^{-1} GM-CSF (Peprotech). After 10 d, the HMDMs were used for experiments.

Cell lines. Jurkat human T lymphocytes (TIB-152) and L-929 mouse fibroblasts (CCL-1) cells were obtained from the American Type Culture Collection and cultured in DMEM (Gibco) supplemented with 10% (v/v) heat-inactivated FBS (Gibco), 10 U ml^{-1} penicillin and 100 mg ml^{-1} streptomycin (Corning). Cells were cultured in a humidified CO_2 incubator at 37 °C.

Induction of apoptosis and labelling of Jurkat cells. Jurkat cells were irradiated under a 254-nm UV lamp for 15 min, followed by incubation in 1× PBS for 2–3 h, and then used for experiments. For some experiments, the ACs were rinsed once with serum-free DMEM, resuspended at a concentration of 2×10^7 cells per ml in Diluent C (Sigma-Aldrich), and incubated for 5 min with 1 ml of Diluent C containing concentrated PKH26 dye (Sigma-Aldrich). The reaction was stopped with 2 ml of FBS, and the ACs were then rinsed twice with DMEM containing 10% heat-inactivated FBS and used for experiments. For other experiments, ACs were stained with pHrodo dye (Thermo Fisher Scientific) as described by the manufacturer's protocol. For experiments using apoptotic human macrophages, HMDMs were made apoptotic by treatment with 1 µM staurosporine in DMEM media for 48 h.

In vitro macrophage efferocytosis assay. BMDMs were plated in 24-well tissue culture plates and incubated with PHK26- or pHrodo-labelled Jurkat cells rendered apoptotic by 254 nM UV at a ratio of 5:1 (ACs/Mϕ, where Mϕ denotes macrophage). After 45 min, unbound ACs were vigorously washed off and fluorescence and bright field images were taken using an epifluorescence microscope (Leica DMI6000B) to identify the uptake of labelled cells. Images were quantified using Image J software. For some experiments, Mϕ were incubated with ACs for 3 h, whereas other experiments involved incubating Mϕ for an additional 1 or 6 h in normal cell culture media following the removal of unbound ACs.

Immunoblotting. After experiments, cells were lysed in 2× Laemmli lysis buffer (Bio-Rad) containing 50 mM dithiothreitol. Lysates were heated at 95 °C for 5 min, separated on 4%–20% SDS–PAGE gradient gels (Invitrogen) at 120 V for 2 h, and electrotransferred to 0.45-mm polyvinylidene difluoride membranes at 100 V for 1.5 h. The membranes were incubated at 4 °C with primary antibodies in PBS containing 5% BSA overnight and detected using horseradish peroxidase-conjugated secondary antibodies (Pierce) the following day. Densitometric analysis was performed using ImageJ software.

Enzyme-linked immunosorbent assay. TGF-β1 or PGE_2 were measured in cell culture media or peritoneal exudates using kits purchased from Biolegend and Cayman Chemicals, respectively, and conducted as described by the manufacturer's protocol.

Methylated DNA capture. Control and H-DNMT3A-KO macrophages were incubated with ACs for 45 min. Noninternalized ACs were removed by media removal and monolayer rinsing, and the macrophages were incubated in fresh media for an additional 1 h. The macrophages were then harvested, and DNA was isolated using the PureLink Genomic DNA Kit (Thermo Fisher Scientific). Next, using 1 µg of DNA from each sample, methylated DNA was captured and detected by antibodies using the Methylamp Methylated DNA Capture Kit from EPIGENTEK, following the manufacturer's protocol. PCR was conducted using primers targeting the CpG-rich region in the promoter of *Dusp4*, and the data were quantified as fold-enrichment of methylated DNA in the *Dusp4* promoter relative to control IgG antibodies that do not recognize methylated DNA.

Short interfering RNA (siRNA)-mediated gene silencing. Scrambled 50 nM siRNA controls or siRNAs targeting specific genes were transfected into macrophages using Lipofectamine RNAiMAX (Life Technologies) following the manufacturer's protocol. Briefly, cells seeded in 450 µl of BMDM media were incubated with 50 µl of OptiMEM containing 1.5 µl of iMAX and 50 nM siRNA. After 48 or 72 h of transfection, experiments were conducted.

Quantitative real-time PCR. RNA was extracted from samples using the PureLink RNA Mini Kit (Life Technologies) following the manufacturer's protocol. The purity and concentration of RNA were determined using a NanoDrop spectrophotometer (Thermo Fisher Scientific). Complementary DNA was synthesized from 200 ng of RNA from samples with a 260/280 ratio >1.8 using oligo(dT) and Superscript II (Applied Biosystems). Quantitative real-time PCR was performed using a 7500 Real-Time PCR system (Applied Biosystems) and SYBR Green Master Mix reagents (Applied Biosystems). All sequences for primers and RNA interference are given in Supplementary Table 1.

Zymosan-induced peritonitis and uptake of apoptotic neutrophils. Male mice (8–10 weeks old) were injected i.p. with 1 ml of 1 mg ml^{-1} Zymosan A (Sigma-Aldrich) to induce sterile peritonitis. For some experiments, mice received 200 ng ml^{-1} recombinant TGF-β1 at 15 and 20 h after Zymosan A injection. Exudate fluid was collected and assayed for TGF-β1 and PGE_2 by enzyme-linked immunosorbent assay (ELISA), and cells in the exudate were stained with mouse anti-Ly6g (neutrophils; Biolegend) and assayed by flow cytometry to quantify neutrophil numbers. To assay apoptotic neutrophil uptake by flow cytometry, exudate cells were stained with anti-F4/80 antibody (macrophages; Biolegend), permeabilized (below) and stained with anti-Gr1. Macrophages that had engulfed apoptotic neutrophils were identified as F4/80$^+$Gr1$^+$ cells.

Flow cytometry. Cells were fixed in 4% PFA (Thermo Fisher Scientific), suspended in FACS staining buffer (PBS containing 2% FBS and 1 mM EDTA), and incubated with TruStain FcX PLUS (anti-mouse CD16/32) Fc-blocking antibody (Biolegend). Cell-surface receptor staining was carried out by incubating with fluorescent antibodies for 60 min at 4 °C. For intracellular staining, cells were permeabilized with BD Perm/Wash (BD Biosciences), followed by fluorescent antibody staining at 4 °C for 1 h. Cells were washed in FACS buffer twice and then resuspended for analysis on a BD FACS Canto II flow cytometer. For detection of apoptosis, cells were washed twice with cold FACS buffer, resuspended in annexin V-binding buffer at a concentration of 1×10^6 cells per ml, and incubated with fluorescein isothiocyanate (FITC)-conjugated annexin V antibody for 15 min at room temperature. Samples were analysed by BD FACS Canto II flow cytometer. Data analysis was carried out using the FlowJo v.10.

Dexamethasone thymus experiment. Male mice (8–10 weeks old) were injected i.p. with 250 µl of PBS containing 250 mg of DEX (Sigma-Aldrich) dissolved in dimethyl sulfoxide. Eighteen hours after injection, the mice were euthanized, and thymi were harvested and weighed. One lobe of the thymus was mechanically disaggregated, and cell number was determined using Countess II (Invitrogen). Then 1×10^6 cells were stained with either FITC-conjugated annexin V antibody (Biolegend) or anti-F4/80 antibody (Biolegend) to determine AC and macrophage number, respectively. The other thymus lobe was formalin-fixed, paraffin-embedded and sectioned, followed by immunostaining the sections with TUNEL reagent (Roche), anti-TGF-β1 (Abcam), anti-p-ERK1/2 (Cell Signaling), anti-DUSP4 (Abcam) and/or anti-Mac2 antibodies (Cedarlane). In situ efferocytosis was quantified by counting TUNEL$^+$ cells that were associated with Mac2$^+$ cells versus macrophage-free TUNEL$^+$ cells. Macrophage-associated ACs followed the criteria of TUNEL$^+$ nuclei surrounded by or in contact with neighbouring Mac2$^+$ macrophages. Free ACs exhibited nuclear condensation and were not in contact with neighbouring macrophages.

Tissue collection and lesion analysis. Male *Ldlr*$^{-/-}$ mice (8–10 weeks/old) were prepared 1 week before irradiation by giving them acidic water containing 100 mg L^{-1} neomycin and 10 g L^{-1} polymyxin. The mice were given 1,000 rads using a caesium-137 Gammacell source. Some 4–6 h later, the mice were injected intravenously with 2.5×10^6 BM cells from 8–10-week-old male control *Vav1Cre*$^{+/-}$ mice or *Dnmt3a*$^{fl/fl}$ *Vav1Cre*$^{+/-}$ mice[56]. Femurs from the donor mice were flushed with RPMI-1640 containing 10 units ml^{-1} heparin, 10 U ml^{-1} penicillin and 100 mg ml^{-1} streptomycin to collect the BM cells, which were then passed through a 40-mm cell strainer, collected by centrifugation at 500*g* for 5 min, and washed twice before loading into a syringe for injection. Four weeks after injection of BM cells, mice were fed a western-type diet (Envigo, TD 88137) for 12 weeks. The work-up of the mice and all atherosclerosis measurements were conducted as described previously[6,33]. In brief, the night before the mice were euthanized, food was withdrawn, and the next morning blood glucose was assayed using a OneTouch Ultra device, plasma cholesterol was measured using a kit from Wako Diagnostics, and complete blood cell counts and leucocyte differential were quantified using a FORCYTE Hematology Analyzer (Oxford Science). The mice were then euthanized, followed by PBS perfusion through the left ventricle. Aortic roots were formalin-fixed, paraffin-embedded, sectioned and stained with haematoxylin and eosin[6,33]. For each mouse, we quantified six sections that were separated by 30 mm, starting at the base of the aortic root. The area from the internal elastic lamina to the lumen (total lesion area) was quantified using image analysis software. The lesions were also stained for collagen using picrosirius red (Polysciences, catalogue no. 24901A) to quantify fibrous cap thickness at the cap midpoint and both shoulder regions. These measurements were averaged and expressed as the ratio of collagen cap thickness to lesion area.

Tissue immunohistochemistry and immunofluorescence microscopy. Paraffin-embedded sections (6 mm) were deparaffinized with xylene and rehydrated in decreasing concentrations of ethanol. Sections were incubated with TUNEL staining reagents at 37 °C for 60 min and then washed three times with PBS. Alternatively, rehydrated sections were blocked for 60 min with 2% BSA in 1× PBS, and immunostained with anti-Mac2, anti-COX2, anti-TGF-β1 or anti-DUSP4 antibodies overnight at 4 °C. Sections were stained with fluorescently labelled secondary antibodies and then counterstained with 4,6-diamidino-2-phenylindole. Images were captured using an epifluorescence microscope (Leica DMI6000B).

Detection of $^{13}C_5{}^{15}N$-labelled SAM in BMDMs incubated with ACs labelled with $^{13}C_5{}^{15}N$-methionine. Jurkat cells incubated with media containing $^{13}C_5{}^{15}N$-methionine were labelled with fluorescent PKH26 dye and then rendered apoptotic. To prevent $^{13}C_5{}^{15}N$-SAM formation in the Jurkat cells themselves, the

cells were pre-incubated with the MAT2A inhibitor PF9366. Next, macrophages were pre-incubated with or without bafilomycin and then incubated with the labelled ACs for 45 min, followed by the removal of unbound ACs by rinsing and further incubation in medium without ACs for 1 h. The macrophages were then sorted into PKH26^{+} (AC^{+}) and PKH26^{-} (AC^{-}) cells and analysed by LC–MS/MS for $^{13}C_5{}^{15}N$-SAM. Briefly, 500 µl of prechilled cold methanol was added to each cell pellet, followed by vortexing and incubation at −80 °C for 20 min. Samples were centrifuged at 14,000*g* for 5 min, and the metabolite extract was collected in a clean microcentrifuge tube. The pellet was re-extracted as described above, and the metabolite extracts were pooled, dried in a vacuum centrifuge (Savant SC210A SpeedVac Concentrator, Thermo Fisher Scientific), and resuspended in liquid chromatography loading solvent. For isotope tracer analysis, an ultra-high performance liquid chromatograph (Vanquish, Thermo Fisher Scientific) interfaced with an electrospray Q Exactive Focus mass spectrometer (Thermo Fisher Scientific) was used in full scan mode. The following solvent systems were used: solvent A was 100% LC–MS grade water (Burdick & Jackson) containing 0.1% formic acid (Thermo Fisher Scientific, catalogue no. 28905), and solvent B was aqueous 100% LC–MS grade acetonitrile (Burdick & Jackson, catalogue no. 34967). For each sample, a 5-µl aliquot of the metabolite mixture was loaded onto an ACE C18-PFP column, (2.1 mm internal diameter (i.d.) × 100 mm length with 2 µm particle size). The column was equilibrated at 0% B with a flow rate of 0.350 ml min^{-1} for 3 min. A gradient from 0% B to 80% B was applied over 10 min with a flow rate of 0.350 ml min^{-1}, held at 80% B for 3 min, followed by re-equilibration over 5 min, giving a total of 21 min for the LC experiment. Mass spectrometry (MS) instrument parameters for full Scan MS on the Q Exactive Focus included the following: resolution, 70,000; AGC target, 3×10^6; and maximum injection time, 100 ms. Peak heights for unlabelled methionine and SAM and $^{13}C_5{}^{15}N$-labelled methionine and $^{13}C_5{}^{15}N$-labelled SAM were extracted from the chromatograms using Xcalibur Quan Browser (v.4.2.47, Thermo Fisher Scientific).

Detection and quantification of ^{13}C-CH_3 in genomic DNA. Macrophages pretreated with or without bafilomycin and/or PF9366 were incubated for 45 min with or without $^{13}C_5{}^{15}N$-methionine-labelled Jurkat cells (above). Unengulfed ACs were removed by rinsing and then incubated for an additional 1 h. DNA was extracted from the cells and digested into single nucleosides by incubation with the Nucleoside Digestion Mix (New England Biolabs) at 37 °C for 2 h. ^{13}C-DNA methylation was identified and quantified by nano-liquid chromatography (nLC) coupled online with <S. nLC was configured with a two-column system consisting in a 300 µm i.d. × 0.5 cm C18 trap column (Dionex) and a 75 µm i.d. × 25 cm Reprosil-Pur C18-AQ (3 µm; Dr Maisch GmbH) analytical nano-column packed in-house using a Dionex RSLC Ultimate 3000 (Thermo Fisher Scientific). nLC was coupled to an Orbitrap Fusion Lumos mass spectrometer (Thermo Fisher Scientific). The voltage of the spray was set to 2.3 kV, and the temperature of the heated capillary was set to 275 °C. A full scan range of 110–600 *m*/*z* was acquired in the Orbitrap at a resolution of 120,000. The source fragmentation energy was set at 30 V, and the RF lens was set at 50%. The instrument was optimized to fragment the protonated nucleosides deoxy-methylcytidine and labelled ^{13}C-deoxy-methylcytidine into protonated nucleobases mC and ^{13}C-mC with *m*/*z* at 126.0662 and 127.0695, respectively. The percentage of ^{13}C-labelled methylation was calculated using the intensity of mC over mC + ^{13}C-mC.

Statistical analysis. GraphPad Prism software (v.9.2.0) was used for all statistical analyses. We first subjected data to the D'Agostino–Pearson or Shapiro–Wilk test and found that all data were normally distributed. For comparison of two groups, we used the Student's *t*-test to calculate *P* values, and for more than two groups we used one-way analysis of variance (ANOVA) with Fisher's least significant difference (LSD) post hoc analysis. Data are reported as means ± s.e.m., and differences were considered statistically significant at $P < 0.05$. Using power calculations based on our previous studies in mice using the DEX-thymus, Zymosan peritonitis and mouse atherosclerosis models, the numbers of mice chosen for each cohort were sufficient to enable the testing of our hypotheses based on an expected 20%–30% coefficient of variation and an 80% chance of detecting a 33% difference in key plaque parameters (lesion size and fibrous cap thickness). Before the start of any analyses, mice were excluded if they died, suffered an injury requiring euthanasia, or lost >15% of their body weight.

Reporting Summary. Further information on research design is available in the Nature Research Reporting Summary linked to this article.

Data availability

This study did not generate any unique datasets or codes. All other data can be made available from the authors on reasonable request. Additional data associated with the paper can be found in the Supplementary Information. Source data are provided with this paper.

Received: 2 August 2021; Accepted: 11 February 2022;
Published online: 31 March 2022

References

1. Dalli, J. & Serhan, C. N. Pro-resolving mediators in regulating and conferring macrophage function. *Front. Immunol.* **8**, 1400 (2017).
2. Doran, A. C., Yurdagul, A. Jr & Tabas, I. Efferocytosis in health and disease. *Nat. Rev. Immunol.* **20**, 254–267 (2020).
3. Morioka, S., Maueroder, C. & Ravichandran, K. S. Living on the edge: efferocytosis at the interface of homeostasis and pathology. *Immunity* **50**, 1149–1162 (2019).
4. Linton, M. F. et al. Macrophage apoptosis and efferocytosis in the pathogenesis of atherosclerosis. *Circ. J.* **80**, 2259–2268 (2016).
5. Kojima, Y., Weissman, I. L. & Leeper, N. J. The role of efferocytosis in atherosclerosis. *Circulation* **135**, 476–489 (2017).
6. Yurdagul, A. Jr et al. Macrophage metabolism of apoptotic cell-derived arginine promotes continual efferocytosis and resolution of injury. *Cell Metab.* **31**, 518–533 e510 (2020).
7. Zhang, S. et al. Efferocytosis fuels requirements of fatty acid oxidation and the electron transport chain to polarize macrophages for tissue repair. *Cell Metab.* **29**, 443–456 e445 (2019).
8. A-Gonzalez, N. et al. Apoptotic cells promote their own clearance and immune tolerance through activation of the nuclear receptor LXR. *Immunity* **31**, 245–258 (2009).
9. Fadok, V. A. et al. Macrophages that have ingested apoptotic cells in vitro inhibit proinflammatory cytokine production through autocrine/paracrine mechanisms involving TGF-beta, PGE2, and PAF. *J. Clin. Invest.* **101**, 890–898 (1998).
10. Nakanishi, M. & Rosenberg, D. W. Multifaceted roles of PGE2 in inflammation and cancer. *Semin. Immunopathol.* **35**, 123–137 (2013).
11. Funk, C. D. & FitzGerald, G. A. COX-2 inhibitors and cardiovascular risk. *J. Cardiovasc. Pharmacol.* **50**, 470–479 (2007).
12. Cheng, H., Huang, H., Guo, Z., Chang, Y. & Li, Z. Role of prostaglandin E_2 in tissue repair and regeneration. *Theranostics* **11**, 8836–8854 (2021).
13. Tang, E. H., Libby, P., Vanhoutte, P. M. & Xu, A. Anti-inflammation therapy by activation of prostaglandin EP4 receptor in cardiovascular and other inflammatory diseases. *J. Cardiovasc. Pharmacol.* **59**, 116–123 (2012).
14. Takayama, K. et al. Prostaglandin E_2 suppresses chemokine production in human macrophages through the EP4 receptor. *J. Biol. Chem.* **277**, 44147–44154 (2002).
15. Gitlin, J. M. & Loftin, C. D. Cyclooxygenase-2 inhibition increases lipopolysaccharide-induced atherosclerosis in mice. *Cardiovasc. Res.* **81**, 400–407 (2009).
16. Kirkby, N. S. et al. COX-2 protects against atherosclerosis independently of local vascular prostacyclin: identification of COX-2 associated pathways implicate Rgl1 and lymphocyte networks. *PLoS ONE* **9**, e98165 (2014).
17. Yu, Z. et al. Disruption of the 5-lipoxygenase pathway attenuates atherogenesis consequent to COX-2 deletion in mice. *Proc. Natl Acad. Sci. USA* **109**, 6727–6732 (2012).
18. Narasimha, A. et al. A novel anti-atherogenic role for COX-2–potential mechanism for the cardiovascular side effects of COX-2 inhibitors. *Prostaglandins Other Lipid Mediat.* **84**, 24–33 (2007).
19. Yoshimura, A., Wakabayashi, Y. & Mori, T. Cellular and molecular basis for the regulation of inflammation by TGF-beta. *J. Biochem.* **147**, 781–792 (2010).
20. Mallat, Z. et al. Inhibition of transforming growth factor-beta signaling accelerates atherosclerosis and induces an unstable plaque phenotype in mice. *Circ. Res.* **89**, 930–934 (2001).
21. Martinez, J. et al. Microtubule-associated protein 1 light chain 3 alpha (LC3)-associated phagocytosis is required for the efficient clearance of dead cells. *Proc. Natl Acad. Sci. USA* **108**, 17396–17401 (2011).
22. Mao, Y. et al. Inhibition of tumor-derived prostaglandin-e2 blocks the induction of myeloid-derived suppressor cells and recovers natural killer cell activity. *Clin. Cancer Res.* **20**, 4096–4106 (2014).
23. Sun, W. H. et al. Induction of cyclooxygenase-2 in rat gastric mucosa by rebamipide, a mucoprotective agent. *J. Pharmacol. Exp. Ther.* **295**, 447–452 (2000).
24. Mato, J. M., Martinez-Chantar, M. L. & Lu, S. C. S-adenosylmethionine metabolism and liver disease. *Ann. Hepatol.* **12**, 183–189 (2013).
25. Parkhitko, A. A., Jouandin, P., Mohr, S. E. & Perrimon, N. Methionine metabolism and methyltransferases in the regulation of aging and lifespan extension across species. *Aging Cell* **18**, e13034 (2019).
26. Quinlan, C. L. et al. Targeting S-adenosylmethionine biosynthesis with a novel allosteric inhibitor of Mat2A. *Nat. Chem. Biol.* **13**, 785–792 (2017).
27. Finkelstein, J. D. Pathways and regulation of homocysteine metabolism in mammals. *Semin. Thromb. Hemost.* **26**, 219–225 (2000).
28. Okano, M., Bell, D. W., Haber, D. A. & Li, E. DNA methyltransferases Dnmt3a and Dnmt3b are essential for de novo methylation and mammalian development. *Cell* **99**, 247–257 (1999).
29. Cho, K. N. et al. Prostaglandin E_2 induces MUC8 gene expression via a mechanism involving ERK MAPK/RSK1/cAMP response element binding protein activation in human airway epithelial cells. *J. Biol. Chem.* **280**, 6676–6681 (2005).

30. Xia, Q. et al. Induction of COX-2-PGE2 synthesis by activation of the MAPK/ERK pathway contributes to neuronal death triggered by TDP-43-depleted microglia. *Cell Death Dis.* **6**, e1702 (2015).
31. Xiong, W., Frasch, S. C., Thomas, S. M., Bratton, D. L. & Henson, P. M. Induction of TGF-beta1 synthesis by macrophages in response to apoptotic cells requires activation of the scavenger receptor CD36. *PLoS ONE* **8**, e72772 (2013).
32. Cai, B. et al. Macrophage MerTK promotes liver fibrosis in nonalcoholic steatohepatitis. *Cell Metab.* **31**, 406–421 e407 (2020).
33. Gerlach, B. D. et al. Efferocytosis induces macrophage proliferation to help resolve tissue injury. *Cell Metab.* **33**, 2445–2463 e2448 (2021).
34. Nishi, C., Yanagihashi, Y., Segawa, K. & Nagata, S. MERTK tyrosine kinase receptor together with TIM4 phosphatidylserine receptor mediates distinct signal transduction pathways for efferocytosis and cell proliferation. *J. Biol. Chem.* **294**, 7221–7230 (2019).
35. Lang, R., Hammer, M. & Mages, J. DUSP meet immunology: dual specificity MAPK phosphatases in control of the inflammatory response. *J. Immunol.* **177**, 7497–7504 (2006).
36. Newson, J. et al. Inflammatory resolution triggers a prolonged phase of immune suppression through COX-1/mPGES-1-derived prostaglandin E2. *Cell Rep.* **20**, 3162–3175 (2017).
37. Cai, B. et al. MerTK cleavage limits proresolving mediator biosynthesis and exacerbates tissue inflammation. *Proc. Natl Acad. Sci. USA* **113**, 6526–6531 (2016).
38. Ren, Y. & Savill, J. Proinflammatory cytokines potentiate thrombospondin-mediated phagocytosis of neutrophils undergoing apoptosis. *J. Immunol.* **154**, 2366–2374 (1995).
39. Tse, K. & Ley, K. Transforming growth factor-beta: transforming plaque to stability. *Eur. Heart J.* **34**, 3684–3686 (2013).
40. Takeuch, O. & Akira, S. Epigenetic control of macrophage polarization. *Eur. J. Immunol.* **41**, 2490–2493 (2011).
41. Roy, D. G. et al. Methionine metabolism shapes T helper cell responses through regulation of epigenetic reprogramming. *Cell Metab.* **31**, 250–266. e259 (2020).
42. Ji, J. et al. Methionine attenuates lipopolysaccharide-induced inflammatory responses via DNA methylation in macrophages. *ACS Omega* **4**, 2331–2336 (2019).
43. Shikauchi, Y. et al. SALL3 interacts with DNMT3A and shows the ability to inhibit CpG island methylation in hepatocellular carcinoma. *Mol. Cell. Biol.* **29**, 1944–1958 (2009).
44. Guo, X. et al. Structural insight into autoinhibition and histone H3-induced activation of DNMT3A. *Nature* **517**, 640–644 (2015).
45. Dai, Z., Mentch, S. J., Gao, X., Nichenametla, S. N. & Locasale, J. W. Methionine metabolism influences genomic architecture and gene expression through H3K4me3 peak width. *Nat. Commun.* **9**, 1955 (2018).
46. Fredman, G. et al. An imbalance between specialized pro-resolving lipid mediators and pro-inflammatory leukotrienes promotes instability of atherosclerotic plaques. *Nat. Commun.* **7**, 12859 (2016).
47. Merched, A. J., Ko, K., Gotlinger, K. H., Serhan, C. N. & Chan, L. Atherosclerosis: evidence for impairment of resolution of vascular inflammation governed by specific lipid mediators. *FASEB J.* **22**, 3595–3606 (2008).
48. Takayama, K., Sukhova, G. K., Chin, M. T. & Libby, P. A novel prostaglandin E receptor 4-associated protein participates in antiinflammatory signaling. *Circ. Res.* **98**, 499–504 (2006).
49. Jaiswal, S. et al. Clonal hematopoiesis and risk of atherosclerotic cardiovascular disease. *N. Engl. J. Med.* **377**, 111–121 (2017).
50. Sharma, M. et al. Regulatory T cells license macrophage pro-resolving functions during atherosclerosis regression. *Circ. Res.* **127**, 335–353 (2020).
51. Toussirot, E., Bonnefoy, F., Vauchy, C., Perruche, S. & Saas, P. Mini-Review: The administration of apoptotic cells for treating rheumatoid arthritis: current knowledge and clinical perspectives. *Front. Immunol.* **12**, 630170 (2021).
52. Mevorach, D. et al. Single infusion of donor mononuclear early apoptotic cells as prophylaxis for graft-versus-host disease in myeloablative HLA-matched allogeneic bone marrow transplantation: a phase I/IIa clinical trial. *Biol. Blood Marrow Transpl.* **20**, 58–65 (2014).
53. Zhang, Z. et al. Clearance of apoptotic cells by mesenchymal stem cells contributes to immunosuppression via PGE_2. *EBioMedicine* **45**, 341–350 (2019).
54. Pujol-Autonell, I. et al. Efferocytosis promotes suppressive effects on dendritic cells through prostaglandin E2 production in the context of autoimmunity. *PLoS ONE* **8**, e63296 (2013).
55. Fourgeaud, L. et al. TAM receptors regulate multiple features of microglial physiology. *Nature* **532**, 240–244 (2016).
56. Kasikara, C. et al. Deficiency of macrophage PHACTR1 impairs efferocytosis and promotes atherosclerotic plaque necrosis. *J. Clin. Invest.* e145275 (2021).

Acknowledgements

We thank S. Mukherjee and A. Burke (Columbia University) for the *Dnmt3a*$^{fl/fl}$ *Vav1Cre*$^{+/-}$ mice; R. Bowman and R. Levine (Memorial Sloan Kettering Cancer Center) for initial discussions about the experimental approach using *Dnmt3a*-targeted mice; and J. Wang and X. Huang (Columbia) for initial discussions on DNA methylation assays. We acknowledge C. Lu of the Columbia Center for Translational Immunology Core Facility for assisting in the flow cytometry and immunofluorescent imaging experiments, which were conducted in the Columbia Center for Translational Immunology Core Facility, funded by NIH grants P30CA013696, S10OD020056 and S10RR027050. This study was funded by a Transatlantic Network of Excellence (TNE-18CVD04) grant from the Leducq Foundation (to A.R.T. and I.T.) and by the following NIH grants: R00 DK115778 (to B.C.); T32 5T32HL007343-42 (to B.D.G.); K99 HL145131 (to A.Y.); R01 HL127464 (to I.T.); and R01 HL087123 and R35 HL145228 (to I.T.). B.C. received funding support from R00DK115778. S.S. and Y.S. acknowledge the Leukemia Research Foundation (Hollis Brownstein New Investigator Research Grant); AFAR (Sagol Network GerOmic Award); the Einstein Nathan Shock Center for the Biology of Aging, Deerfield (Xseed award); NIH P30 grant CA01333047; shared instrument grant NIH 1 S10 OD030286-01; and NIGMS grant 5 R01GM129350-04 (PI: Brenowitz). This work has also been supported in part by the Proteomics & Metabolomics Core Facility at the H. Lee Moffitt Cancer Center & Research Institute, an NCI designated Comprehensive Cancer Center (P30-CA076292).

Author contributions

P.B.A. and I.T. developed the study concept and experimental design. Key advice was provided by A.R.T., P.B.A., B.C. and S.S. P.B.A., S.R.S. and B.D.G. conducted the experiments. X.W., A.Y. and G.K. assisted with bone marrow transplants, Zymosan A1-induced peritonitis experiments, dexamethasone-induced thymocyte apoptosis experiments and atherosclerosis experiments. L.N.F.D. carried out analysis of intracellular $^{13}C_5{}^{15}N$-methionine and $^{13}C_5{}^{15}N$-SAM in macrophages under the guidance of J.M.K. Y.S. conducted the experiments to detect ^{13}C-labelled DNA in macrophages under the guidance of S.S. P.B.A. and I.T. wrote the manuscript and the other co-authors provided comments and revisions.

Competing interests

The authors declare no competing interests.

Additional information

Extended data is available for this paper at https://doi.org/10.1038/s42255-022-00551-7.

Supplementary information The online version contains supplementary material available at https://doi.org/10.1038/s42255-022-00551-7.

Correspondence and requests for materials should be addressed to Patrick B. Ampomah or Ira Tabas.

Peer review information *Nature Metabolism* thanks Derek W. Gilroy, Xiaoling Li and the other, anonymous, reviewers for their contribution to the peer review of this work. Primary Handling Editor: Isabella Samuelson.

Reprints and permissions information is available at www.nature.com/reprints.

Publisher's note Springer Nature remains neutral with regard to jurisdictional claims in published maps and institutional affiliations.

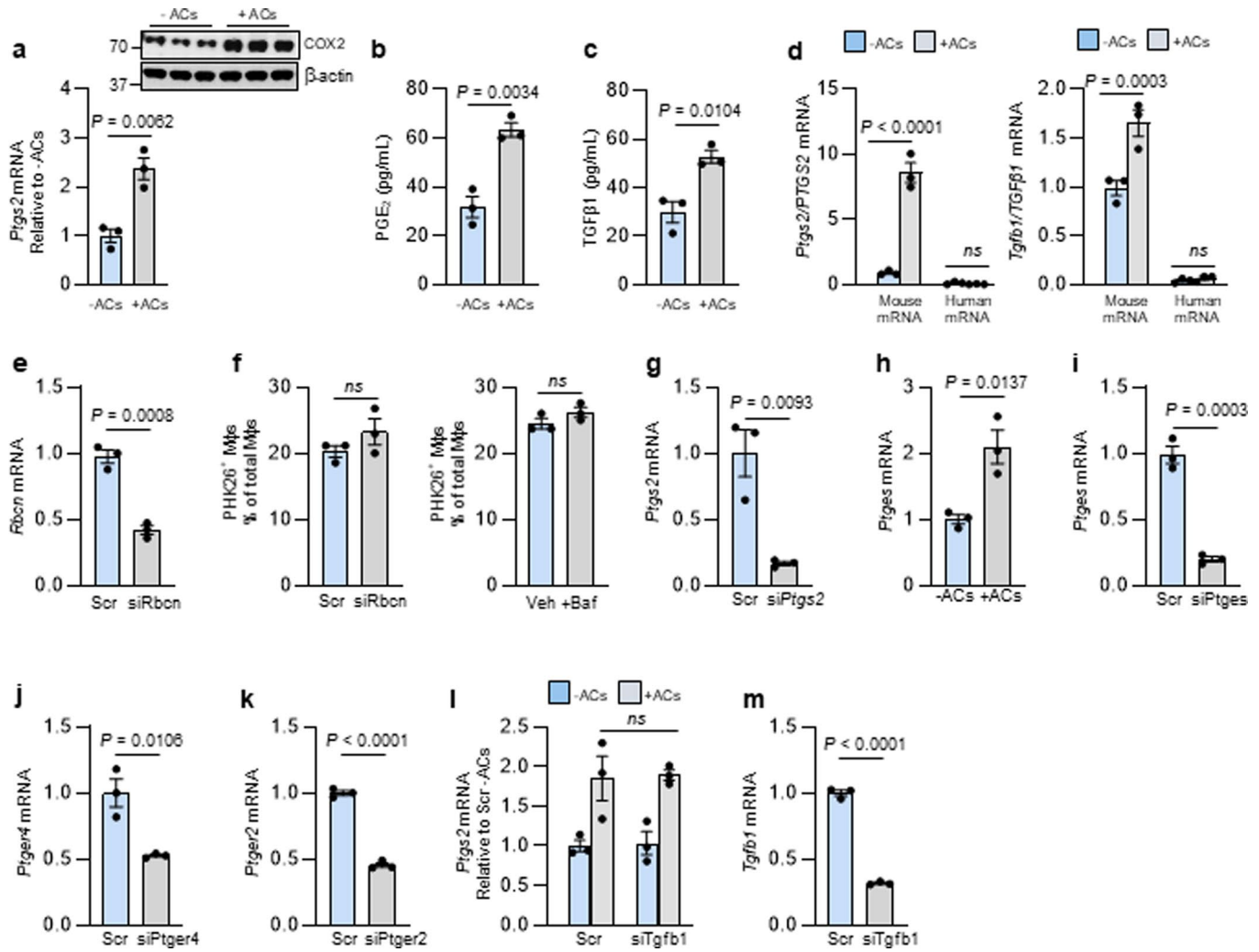

Extended Data Fig. 1 | Additional experiments documenting the efferocytosis-*Ptgs2*/COX2-TGFβ1 pathway in macrophages. Related to Fig. 1. BMDMs were incubated ± ACs, after which noninternalized ACs were removed by rinsing. The cells were assayed for *Ptgs2* mRNA after an additional 1 h incubation and COX2 protein after 3 h (**a**); PGE_2 in the media after 3 h (**b**); and TGFβ1 in the media after 18 h (**c**). For (**d**), experiments similar to those in panel a were analyzed for mouse and human *Ptgs2/PTGS2* or *Tgfb1/TGFβ1* mRNA to prove that mRNA being measured is not residual human mRNA derived from human apoptotic Jurkat cells. **e**, BMDMs were transfected with scrambled RNA (Scr) or siRbcn and then, after 72 h, assayed for *Rbcn* mRNA. **f**, BMDMs were transfected with Scr or siRbcn or treated with vehicle or bafilomycin A1 and then incubated with PKH26-labelled ACs for 45 min, followed by rinsing and quantification of percent $PKH26^+$ macrophages of total macrophages. **g**, BMDMs were transfected with Scr or siPtgs2 and then, after 72 h, assayed for *Ptgs2* mRNA. **h**, BMDMs were incubated ± ACs for 45 min, after which noninternalized ACs were removed by rinsing. The cells were assayed for *Ptges* mRNA after an additional 1 h incubation. **i**, BMDMs were transfected with scrambled RNA (Scr) or siPtges and then, after 72 h, assayed for *Ptges* mRNA. **j-k**, BMDMs were transfected with Scr, siPtger4, or siPtger2 and then, after 72 h, assayed for *Ptger4* or *Ptger2* mRNA, respectively. **l**, BMDMs were transfected with Scr or siTgfb1. After 72 h, the cells were incubated ± ACs for 45 min, after which noninternalized ACs were removed by rinsing. After an additional 1 h of incubation, the cells were assayed for *Ptgs2* mRNA. **m**, BMDMs were transfected with Scr or si*Tgfb1* and then, after 72 h, assayed for *Tgfb1* mRNA. All mRNA data are expressed relative to the first control group. Values are means ± SEM. *ns*, not significant ($P > 0.05$); n = 3 biological replicates. Two-sided *P* values were determined by a Student's t-test for two groups or one-way ANOVA with Fisher's LSD posthoc analysis for three or more groups.

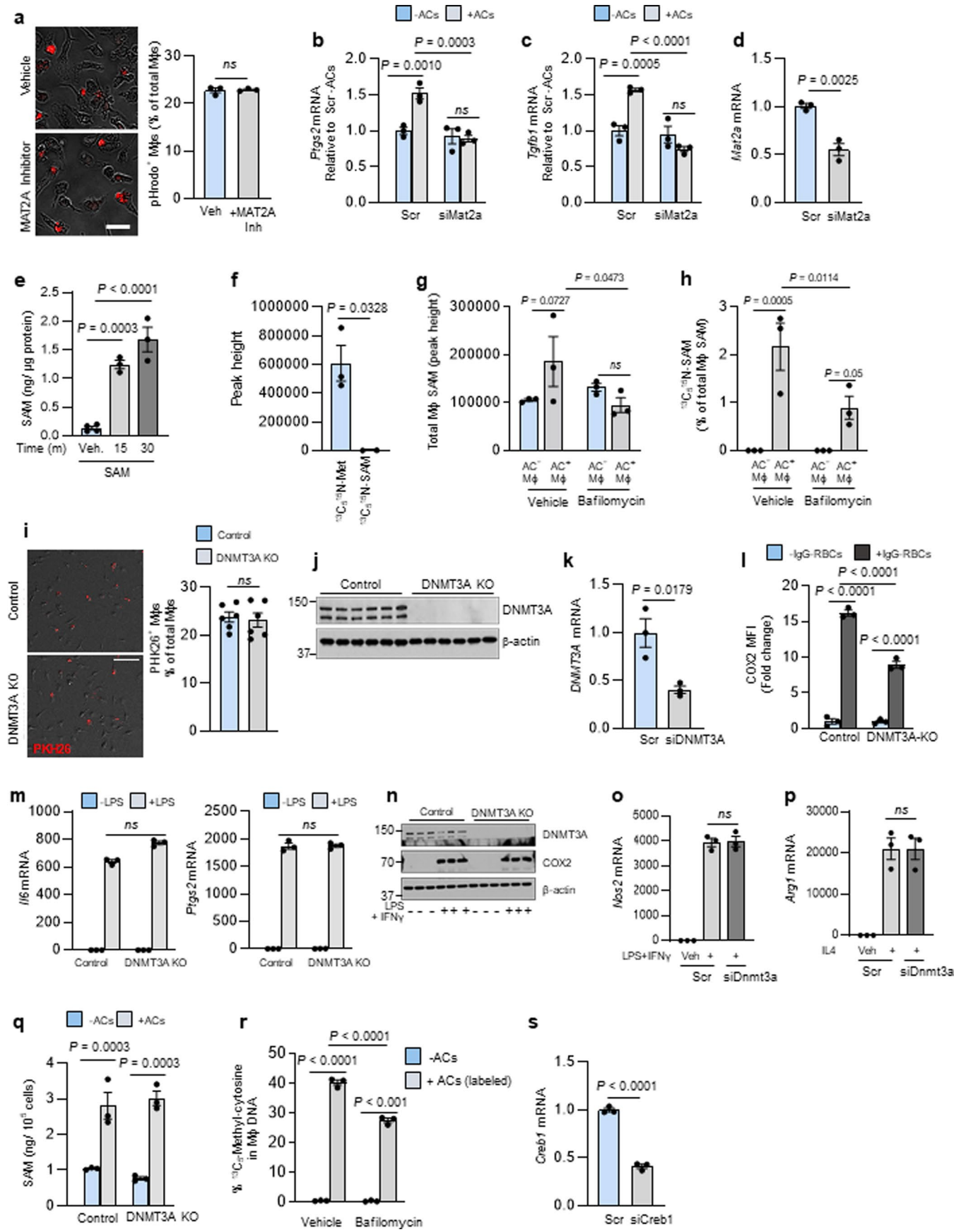

Extended Data Fig. 2 | See next page for caption.

Extended Data Fig. 2 | Additional experiments documenting the role of SAM in the efferocytosis-*Ptgs2*/COX2-TGFβ1 pathway. Related to Figs. 2 & 3. All AC incubations were 45 min, and *Ptgs2* or *Tgfb1* were assayed 1 or 6 h after AC removal, respectively. **a**, BMDMs pretreated 2 h with vehicle or the MAT2A inhibitor PF9366 were incubated with pHrodo-labeled ACs and quantified for the percent pHrodo-AC$^+$ macrophages. Scale bar, 50 μm. **b-c**, BMDMs treated with scrambled RNA (Scr) or siMat2a were incubated ± ACs and then assayed for *Ptgs2* or *Tgfb1*. **d**, BMDMs treated with Scr or siMat2a were assayed for *Mat2a*. **e**, BMDMs treated with vehicle or SAM were assayed for SAM content. **f**, Jurkat cells were cultured in methionine-free DMEM supplemented with dialyzed FBS containing 13C515N-methionine and the MAT2A inhibitor, PF9366. The cells were rendered apoptotic after the third day of culture and analyzed by LC-MS/MS to show accumulation of 13C515N-methionine in the presence of MAT2A inhibitor, expressed as peak height, BMDMs cultured in methionine-free media with D-FBS and pretreated for 2 h with vehicle or bafilomycin A1 (Baf) were incubated 1 h with PKH26-labeled ACs whose proteins were labeled with $^{13}C_5{}^{15}N$-methionine. AC$^+$ and AC$^-$ macrophages were sorted and assayed for SAM content (**g**) and percent $^{13}C_5{}^{15}N$-SAM of total SAM (**h**). **i**, Control or DNMT3A-KO BMDMs were incubated with PKH26–labelled ACs and then quantified for the percent PKH26-AC$^+$ macrophages. Scale bar, 50 μm. **j**, Control and DNMT3A-KO BMDMs were immunoblotted for DNMT3A and β-actin. **k**, HMDMs treated with Scr or siDNMT3A were assayed for *DNMT3A*. **l**, BMDMs were incubated with IgG-coated RBCs for 45 min and then assayed 3 h later for COX2 MFI by flow cytometry. **m-n**, Control and DNMT3A-KO BMDMs treated with LPS or LPS + IFNγ for 4 h were assayed for *Il6*, *Ptgs2*, or COX2 (n). **o-p**, BMDMs treated with Scr or siDnmt3a were incubated for 24 h with vehicle and LPS + IFNγ or IL4 and assayed for *Nos2* or *Arg1*. **q**, Control and DNMT3A-KO BMDMs were incubated ± ACs for 45 min and then assayed for SAM. **r**, BMDMs pretreated for 2 h with vehicle or bafilomycin A1 were incubated ± ACs whose proteins were labeled with $^{13}C_5{}^{15}N$-methionine and then assayed 1 h after AC removal for $^{13}C_5$-mC in DNA. **s**, BMDMs treated with Scr or siCreb1 were assayed for *Creb1*. All mRNA data are expressed relative to the first control group. Values are means ± SEM. *n.s.*, not significant ($P > 0.05$); n = 3 biological replicates for all bar graphs except i (n = 6). Two-sided *P* values were determined by the Student's t-test for two groups or one-way ANOVA with Fisher's LSD posthoc analysis for three or more groups.

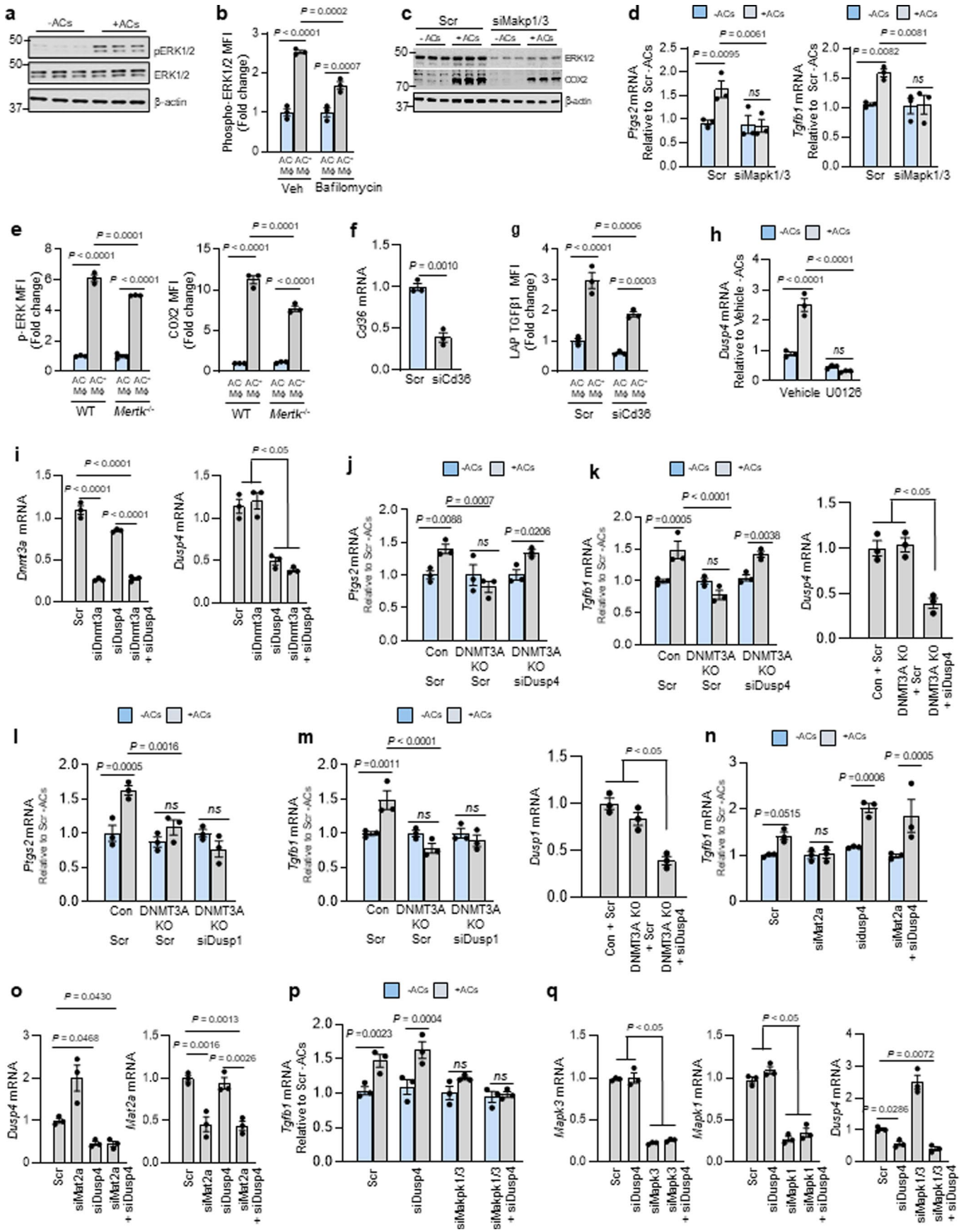

Extended Data Fig. 3 | See next page for caption.

Extended Data Fig. 3 | Experiments documenting the role of ERK, CD36, and DUSP4 in the efferocytosis-*Ptgs2*/COX2-TGFβ1 pathway. Related to Fig. 4. AC incubations were 45 min, and *Ptgs2* or *Tgfb1* were assayed 1 or 6 h after AC removal, respectively. **a**, BMDMs incubated ± ACs were immunoblotted for p-ERK1/2, ERK1/2, and β-actin. **b**, BMDMs pretreated with vehicle or bafilomycin A1 were incubated ± PKH26-labelled ACs for 45 min and assayed by flow cytometry for p-ERK1/2 in PKH26^{+} (AC^{+}) and PKH26^{-} (AC^{-}) macrophages. **c-d**, BMDMs transfected with scrambled RNA (Scr) or siMapk1 and siMapk3 were incubated ± ACs for 45 min and immunoblotted for ERK1/2, COX2, and β-actin or assayed for *Ptgs2* or *Tgfb1*. **e**, WT or MerTK-KO BMDMs were incubated with PKH26-labelled ACs and assayed by flow cytometry for p-ERK1/2 or, after a 3-h chase, COX2. (**f**) BMDMs treated with Scr or si*Cd36* were assayed for *Cd36*. **(g)** BMDMs treated with Scr or siCd36 were incubated with pHrodo–labelled ACs and, after an 18-h chase, assayed by flow cytometry for TGFβ1 in pHrodo^{+} (AC^{+}) and pHrodo^{-} (AC^{-}) macrophages. **h**, BMDMs pretreated for 2 h with vehicle or U0126 (MEK inhibitor) were incubated ± ACs and assayed for *Dusp4*. **i**, BMDMs treated with Scr, siDnmt3a, siDusp4, or siDnmt3a + siDusp4 were assayed for *Dnmt3a* or *Dusp4*. **j-k**, Control or DNMT3A-KO BMDMs transfected with Scr or siDusp4 as indicated were incubated ± ACs and assayed for *Ptgs2* or *Tgfb1*. **l-m**, Control or DNMT3A-KO BMDMs treated with Scr or siDusp1 as indicated were incubated ± ACs and assayed for *Ptgs2* or *Tgfb1*. **n-o**, BMDMs treated with Scr, siMat2a, siDusp4, or siMat2a + siDusp4 were incubated ± ACs and assayed for *Tgfb1*. **p-q**, BMDMs treated with Scr, siMapk1/3, siDusp4, or siMapk1/3 + siDusp4 were incubated ± ACs and assayed for *Tgfb1*, *Mapk3*, *Mapk1*, and *Dusp4* after a 6-h chase. Data are expressed relative to the first control group. Values are means ± SEM. *n.s.*, not significant ($P > 0.05$); n = 3 biological replicates. Two-sided *P* values were determined by the Student's t-test for two groups or one-way ANOVA with Fisher's LSD posthoc analysis for three or more groups.

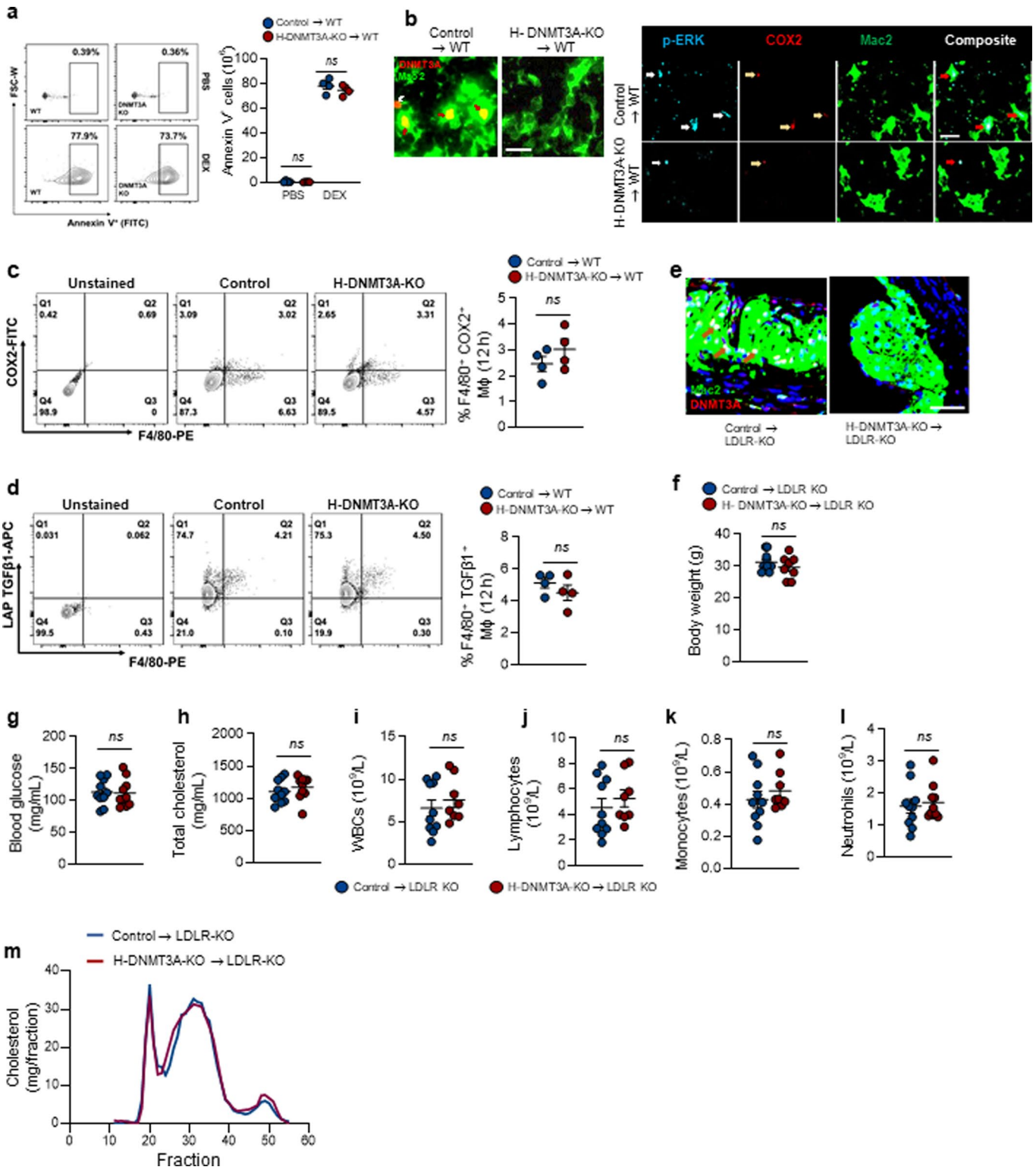

Extended Data Fig. 4 | See next page for caption.

Extended Data Fig. 4 | In vivo evidence of AC—induced COX2-TGFβ1 pathway. Related to Fig. 5. Wild-type (WT) C57BL/6 J mice were transplanted with bone marrow from *Vav1Cre*$^{+/-}$ (Control) or *Dnmt3a*$^{fl/fl}$ *Vav1Cre*$^{+/-}$ (H-DNMT3A-KO) mice and, after 4 weeks, injected with PBS or dexamethasone (DEX). After 4 h, the thymus was harvested and immunostained with anti-annexin V to document the initial increase in apoptosis after PBS or DEX injection, n = 4 mice per group (**a**). For **b** (left), thymi were immunostained with Mac2 (green) and DNMT3A (Red). White arrows indicate non-macrophage DNMT3A, and brown arrows indicate macrophage DNMT3A. For **b** (right), documentation of co-localized p-ERK1/2, COX2, and Mac2. Representative image from n = 4 mice per group. Scale bar, 50 μm. **c-d**, Wildtype (WT) C57BL/6 J mice transplanted with bone marrow from control or H-DNMT3A-KO mice were injected i.p. with 1 mg/mL Zymosan A1. After 12 h, peritoneal exudate cells were analyzed by flow cytometry for F4/80^{+} and COX2^{+} cells (n = 4 mice/group) LAP-TGFβ1^{+} cells (n = 4 mice/group). **e-m**, *Ldlr*$^{-/-}$ (LDLR-KO) mice were transplanted with bone marrow from control or H-DNMT3A-KO mice and, after 4 weeks, fed a western-type diet (WD) for 12 weeks. Aortic root sections were immunostained for Mac2 and DNMT3A. Brown arrows indicate macrophage DNMT3A. Representative image from n = 8 mice per group (**e**); body weight, n = 10 mice/group (**f**); and the plasma or blood was assayed for the indicated metabolic and immune cell parameters, n = 10 mice/group (**g-l**) and the lipoprotein-cholesterol profile by FPLC (**m**). Scale bar, 50 μm. Values are means ± SEM; *n.s.*, not significant ($P > 0.05$). Two-sided *P* values were determined by the Student's t-test for two groups or one-way ANOVA with Fisher's LSD posthoc analysis for three or more groups.

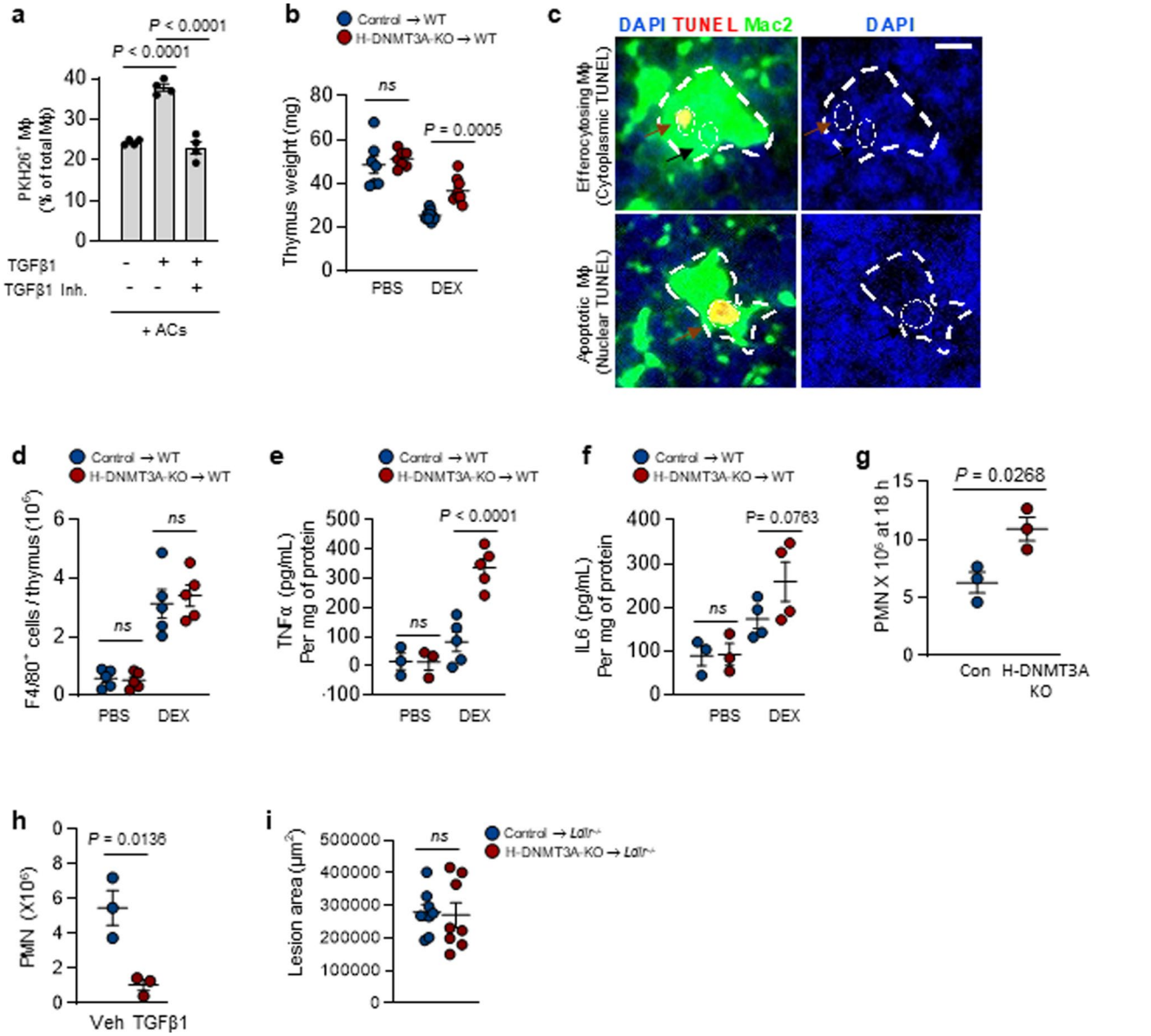

Extended Data Fig. 5 | DNMT3A mediates efferocytosis and resolution in vivo. Related to Fig. 6. BMDMs were pretreated with vehicle or a TGFβ1R inhibitor for 2 h and with vehicle or recombinant TGFβ1 for 1 h, as indicated. The macrophages were then incubated with PKH26–labelled ACs for 45 mins, followed by rinsing and quantification of percent PKH26-AC$^+$ macrophages of total macrophages, n = 4 biological replicates. **b-f**, Wildtype (WT) C57BL/6 J mice were transplanted with bone marrow from control or H-DNMT3A-KO mice and, after 4 weeks, injected with PBS or dexamethasone (DEX). After 18 h, the thymi were weighed, n = 7 and 9 mice for PBS and DEX groups respectively (**b**); immunostained for DAPI, TUNEL, and Mac2 (**c**); assayed for F4/80$^+$ cells, n = 5 mice per group (**d**); and assayed for TNF-a, n = 3 and 5 mice for PBS and DEX groups respectively and IL-6 by ELISA, n = 3 and 4 mice for PBS and DEX groups respectively (**e-f**). The image in b illustrates thymic macrophages with cytoplasmic TUNEL as an example of efferocytosing thymic macrophages. Scale bar, 100 μm. **g**, The peritoneal exudates were assayed for Ly6G$^+$ polymorphonuclear cells (PMN) 18 hours after Zymosan A1 injection, n = 3 mice per group. **h**, Wild-type mice received 200 ng/mL recombinant TGFβ1 i.p. or vehicle control 15 and 20 hours after Zymosan injection and then assayed for the number of PMNs 4 hours later, n = 3 mice/group. **i**, *Ldlr*$^{-/-}$ (LDLR-KO) mice were transplanted with bone marrow from control or H-DNMT3A-KO mice and, after 4 weeks, fed a western-type diet (WD) for 12 weeks. Aortic root sections were quantified for lesional area, n = 8 mice/group. Values are means ± SEM; *n.s.*, not significant ($P > 0.05$). Two-sided *P* values were determined by the Student's t-test for two groups or one-way ANOVA with Fisher's LSD posthoc analysis for three or more groups.

nature portfolio

Corresponding author(s): Ira Tabas

Last updated by author(s): Aug 13, 2021

Reporting Summary

Nature Portfolio wishes to improve the reproducibility of the work that we publish. This form provides structure for consistency and transparency in reporting. For further information on Nature Portfolio policies, see our Editorial Policies and the Editorial Policy Checklist.

Statistics

For all statistical analyses, confirm that the following items are present in the figure legend, table legend, main text, or Methods section.

n/a	Confirmed	
☐	☒	The exact sample size (*n*) for each experimental group/condition, given as a discrete number and unit of measurement
☐	☒	A statement on whether measurements were taken from distinct samples or whether the same sample was measured repeatedly
☐	☒	The statistical test(s) used AND whether they are one- or two-sided *Only common tests should be described solely by name; describe more complex techniques in the Methods section.*
☒	☐	A description of all covariates tested
☐	☒	A description of any assumptions or corrections, such as tests of normality and adjustment for multiple comparisons
☐	☒	A full description of the statistical parameters including central tendency (e.g. means) or other basic estimates (e.g. regression coefficient) AND variation (e.g. standard deviation) or associated estimates of uncertainty (e.g. confidence intervals)
☐	☒	For null hypothesis testing, the test statistic (e.g. *F*, *t*, *r*) with confidence intervals, effect sizes, degrees of freedom and *P* value noted *Give P values as exact values whenever suitable.*
☒	☐	For Bayesian analysis, information on the choice of priors and Markov chain Monte Carlo settings
☒	☐	For hierarchical and complex designs, identification of the appropriate level for tests and full reporting of outcomes
☒	☐	Estimates of effect sizes (e.g. Cohen's *d*, Pearson's *r*), indicating how they were calculated

Our web collection on statistics for biologists contains articles on many of the points above.

Software and code

Policy information about availability of computer code

Data collection	FACS Canto was used for flow cytometry experiments. Applied Biosystems 7500 Software v2.3 was used for RT-qPCR. Leica microscope was used for immunofluorescent images.
Data analysis	ImageJ 1.53f51 was used for immunofluorescence analysis. FlowJo, v10 was used for flow cytometry analysis. GraphPad Prism, v9.2.0 was used to plot graphs and for statistical analysis.

For manuscripts utilizing custom algorithms or software that are central to the research but not yet described in published literature, software must be made available to editors and reviewers. We strongly encourage code deposition in a community repository (e.g. GitHub). See the Nature Portfolio guidelines for submitting code & software for further information.

Data

Policy information about availability of data

All manuscripts must include a data availability statement. This statement should provide the following information, where applicable:

- Accession codes, unique identifiers, or web links for publicly available datasets
- A description of any restrictions on data availability
- For clinical datasets or third party data, please ensure that the statement adheres to our policy

This study did not generate any unique datasets or codes. All other data can be made available from the authors on reasonable request. Additional data associated with the paper can be found in the Supplementary information. Uncropped gele data are included.

Field-specific reporting

Please select the one below that is the best fit for your research. If you are not sure, read the appropriate sections before making your selection.

☒ Life sciences ☐ Behavioural & social sciences ☐ Ecological, evolutionary & environmental sciences

For a reference copy of the document with all sections, see nature.com/documents/nr-reporting-summary-flat.pdf

Life sciences study design

All studies must disclose on these points even when the disclosure is negative.

Sample size	Previous studies and pilot experiments in the lab form the basis of power calculations for the various studies. Depending on the experiment, calculations indicated that 3-12 mice per group would enable the testing of our hypotheses based on an expected 25-30% coefficient of variation and an 80% chance of detecting a 33% difference in the key specified endpoints (P =0.05)
Data exclusions	Pre-specified exclusion criteria were weight loss>10% of initial body weight or signs of illness or injury requiring euthanasia. According to these pre-specified criteria, the maximum number of mice were typically 0-2.
Replication	All experiments were reproducible as assessed in multiple wells of cells, tissue samples or mice. For in vitro assays, experiments involved three or more biological replicates. 4 or more mice were used for in vivo experiments, sufficient for statistical power calculation. We did not have cases of irreproducibility. Data were subjected to extensive reproducibility in all biological assays.
Randomization	Mice of the same age and similar weight were randomly assigned to experimental and control groups. For in vitro experiments, cells were allocated randomly to study groups. Primary cells were allocated into groups based on target genotype.
Blinding	Investigators were not blinded for in vitro assays and some in vivo experiments since target genotype needed to be predetermined before experiments. Investigators were blinded for atherosclerosis lesion and necrotic size quantifications.

Reporting for specific materials, systems and methods

We require information from authors about some types of materials, experimental systems and methods used in many studies. Here, indicate whether each material, system or method listed is relevant to your study. If you are not sure if a list item applies to your research, read the appropriate section before selecting a response.

Materials & experimental systems

n/a	Involved in the study
☐	☒ Antibodies
☐	☒ Eukaryotic cell lines
☒	☐ Palaeontology and archaeology
☐	☒ Animals and other organisms
☒	☐ Human research participants
☒	☐ Clinical data
☒	☐ Dual use research of concern

Methods

n/a	Involved in the study
☒	☐ ChIP-seq
☐	☒ Flow cytometry
☒	☐ MRI-based neuroimaging

The HMDMs were from buffy coats that we purchased from the NY Blood Center, with donors being completely anonymous and unidentifiable to us. See Methods. This is NOT considered "human research participants" as it is exempted based on Protection of Human Rights Title 45 CFR 46.104, section 4(ii).

Antibodies

Antibodies used	The source, catalogue number, vendors and dilutions of all the antibodies used in this paper have been provided as a supplementary table due to the length of the compiled file
Validation	These are all commercial antibodies with validations available either as proofs or publication references on the manufacturers website

Eukaryotic cell lines

Policy information about cell lines

Cell line source(s)	Human Jurkat T Lymphocyte-ATCC TIB-152 and L-929 mouse fibroblasts (ATCC CCL-1)
Authentication	Not authenticated
Mycoplasma contamination	Not tested
Commonly misidentified lines (See ICLAC register)	No commonly misidentified cell lines were used in this study

Animals and other organisms

Policy information about studies involving animals; ARRIVE guidelines recommended for reporting animal research

Laboratory animals	8-week-old male mice were used for all experiments. C57BL/6J (Stock No. 000664) and LDLR KO (B6.129S7-*Ldlrtm1Her/J*) mice were ordered from Jackson lab. Dnmt3a*fl/fl* Vav1Cre+/- mice were a gift from Dr. Siddhartha Mukherjee and Mertk*fl/fl Lyz2cre* male mice were generated as previously described in methods. All genetically altered mice were C57BL/6J. Mice were housed in standard cages at 22C and under a 12-12 h light-dark cycle in a barrier facility with ad libitum access to water and food.
Wild animals	No wild animals were used in this study
Field-collected samples	No field-collected samples were used in this study
Ethics oversight	Animal protocols used for experiments were approved by Columbia University's institutional animal care and use committee.

Note that full information on the approval of the study protocol must also be provided in the manuscript

.

Flow Cytometry

Plots

Confirm that:

☒ The axis labels state the marker and fluorochrome used (e.g. CD4-FITC).

☒ The axis scales are clearly visible. Include numbers along axes only for bottom left plot of group (a 'group' is an analysis of identical markers).

☒ All plots are contour plots with outliers or pseudocolor plots.

☒ A numerical value for number of cells or percentage (with statistics) is provided.

Methodology

Sample preparation	Detailed description of the sample preparation can be found in the methods section
Instrument	FACS Canto
Software	FlowJo v10
Cell population abundance	Sorting yielded about ~30% AC+ versus ~60% AC- macrophage population. Population purity was verified by staining F4/80 for macrophage population.
Gating strategy	FSC-A/SSC-A gating was used to detect all events. FSC-A/FSC-H was used to select singlets

☒ Tick this box to confirm that a figure exemplifying the gating strategy is provided in the Supplementary Information.